

Enhanced Photocatalytic Activity of MXene/Ferrite Hybrid



Ayesha Tariq

Fall 2015-MS Physics

Reg. No. 00000117002

Supervised by:


Dr. Syed Rizwan Hussain

(Associate Professor)

**DEPARTMENT OF PHYSICS, SCHOOL OF NATURAL SCIENCES (SNS),
NATIONAL UNIVERSITY OF SCIENCES & TECHNOLOGY
(NUST) ISLAMABAD, PAKISTAN**

National University of Sciences & Technology**MS THESIS WORK**

We hereby recommend that the dissertation prepared under our supervision by: AYESHA TARIQ, Regn No. 00000117002 Titled: Enhanced Photocatalytic Activity of MXene/Ferrite Hybrid be accepted in partial fulfillment of the requirements for the award of **MS** degree.

Examination Committee Members1. Name: Dr. Faheem AminSignature: 2. Name: Dr. Mohammad Ali MohammadSignature: 

3. Name: _____

Signature: _____

External Examiner: Dr. Javed Iqbal SaggiSignature: Supervisor's Name: Dr. Syed Rizwan HussainSignature: _____
Head of Department24/07/18_____
Date**COUNTERSIGNED**Date: 24/07/18

Dean/Principal


THESIS ACCEPTANCE CERTIFICATE

Certified that final copy of MS thesis written by Ms. Ayesha Tariq, (Registration No. 00000117002), of School of Natural Sciences has been vetted by undersigned, found complete in all respects as per NUST statutes/regulations, is free of plagiarism, errors, and mistakes and is accepted as partial fulfillment for award of MS/M.Phil degree. It is further certified that necessary amendments as pointed out by GEC members and external examiner of the scholar have also been incorporated in the said thesis.

Signature: _____ 

Name of Supervisor: Dr. Syed Rizwan Hussain

Date: _____ 24/07/18

Signature (HoD): _____ 

Date: _____ 24/07/18

Signature (Dean/Principal): _____ 

Date: _____ 24/07/18

Dedicated
To
My loving Parents

Acknowledgment

I am thankful to my Creator **Allah Subhana-Watala** to have guided me throughout this work at every step and for every new thought. Indeed, I could have done nothing without the priceless help and guidance of Allah.

I would like to express special thanks to my supervisor **Dr. Syed Rizwan Hussain** for his helpful guidance, and advice at every stage of this research work.

I am grateful to the principal of the School of Natural Sciences **Prof. Dr. Habib Nasir** and Head of the Department of Physics **Dr. Rizwan Khalid**, for their suggestions and support throughout the program. I would also like to thank my GEC members **Dr. Faheem Amin** and **Dr. Mohammad Ali Mohammad** for giving valuable suggestions to improve my thesis and research work.

I would also like to thank **Dr. Syed Irfan Ali** for helping me for the characterization of my samples.

Special thanks to all my group fellows.

Table of Contents

| | |
|----------------------------------------------------------------|-----------|
| Abstract | 07 |
| Chapter 1 Introduction | 09 |
| 1.1. Introduction to Nanotechnology..... | 09 |
| 1.2. Applications..... | 10 |
| 1.2.1. Applications of Nanotechnology..... | 10 |
| 1.2.2. Nanomaterials..... | 10 |
| 1.2.3. Types of Nanomaterials..... | 10 |
| 1.2.3.1. Zero-Dimensional (0D)..... | 11 |
| 1.2.3.2. One Dimensional (1D)..... | 11 |
| 1.2.3.3. Two Dimensional (2D)..... | 11 |
| 1.2.3.4. Three Dimensional (3D)..... | 11 |
| 1.3. Properties of Bulk and Nanomaterials..... | 12 |
| 1.4. Multiferroic materials..... | 12 |
| 1.5. Single phase multiferroic material..... | 13 |
| 1.5.1. Bismuth Ferrite..... | 13 |
| 1.5.2. Crystal structure..... | 13 |
| 1.5.3. Drawbacks of Bismuth Ferrite (BiFeO ₃)..... | 14 |
| 1.6. Daily applications of Nanomaterials..... | 14 |
| 1.6.1. Solar cells..... | 15 |
| 1.6.2. Nano electronic devices..... | 15 |
| 1.6.3. Catalytic property and environmental control..... | 16 |
| 1.6.4. Sensing devices..... | 16 |
| 1.6.5. Microelectronic Industry..... | 16 |
| 1.6.6. Display Screens (TV)..... | 17 |
| 1.6.7. Space Exploration..... | 17 |
| Chapter 2 Literature Review | 18 |
| Chapter 3 Synthesis and Characterization Tools | 25 |
| 3.1. Apparatus used..... | 25 |
| 3.2. Chemicals..... | 25 |

| | | |
|------------------|-------------------------------------------------------------------------------------------------|-----------|
| 3.3. | Synthesis route of 2D MXene sheets..... | 25 |
| 3.4. | Synthesis of BFO nanoparticles and synthesis of Gadolinium and Tin doped BFO Nanoparticles..... | 26 |
| 3.5. | Synthesis of BFO/MXene hybrid and Gd and Sn doped BFO (BGFSO/MXene hybrid)..... | 27 |
| 3.6. | Characterization Tools..... | 28 |
| 3.6.1. | X-Ray Diffraction (XRD)..... | 29 |
| 3.6.2. | Scanning electron microscope (SEM)..... | 31 |
| 3.6.3. | UV-vis-spectrometer..... | 33 |
| 3.6.4. | Photoluminescence spectroscopy (PL)..... | 35 |
| 3.6.5. | X-Ray photoelectron spectroscopy (XPS)..... | 36 |
| 3.6.6. | Photocatalytic measurement..... | 36 |
| Chapter 4 | Results and Discussion-I | 38 |
| Part A: | BFO/MXene hybrid..... | 38 |
| 4.1.1. | X-Ray Diffraction (XRD)..... | 38 |
| 4.1.2. | Scanning electron microscope (SEM)..... | 39 |
| 4.1.3. | Energy Dispersive X-ray spectroscopy (EDXS)..... | 40 |
| 4.1.4. | X-Ray Photoelectron Spectroscopy..... | 40 |
| 4.1.5. | Photoluminescence Spectra (PL)..... | 42 |
| 4.1.6. | Photocatalytic activity..... | 42 |
| 4.1.6.1 | Photocatalytic process for Dye Degradation..... | 42 |
| 4.1.6.2 | Photocatalytic Activity of BFO/MXene hybrid..... | 44 |
| Chapter 5 | Results and Discussion-II | 46 |
| Part B: | Sn and Gd doped BFO (BGFSO/MXENE) hybrid..... | 46 |
| 5.1.1. | X-Ray Diffraction (XRD)..... | 46 |
| 5.1.2. | SEM Analysis..... | 47 |
| 5.1.3. | X-Ray photoelectron spectra (XPS) of MXene hybrid..... | 48 |

| | |
|-------------------------------------------------------------|----|
| 5.1.4. Absorbance and Band gap of BGFSO/MXene hybrid..... | 50 |
| 5.1.5. Photoluminescence spectra of BGFSO/MXene hybrid..... | 51 |
| 5.1.6. Photocatalytic activity of BGFSO/MXene hybrid..... | 52 |
| Conclusion | 54 |
| References | 55 |

Abstract

The increase of global industrialization has adversely affected the availability of clean water by introducing various harmful substances such as Organic dyes into the water sources. Since the addition of different Organic pollutants destroys our environment hence, the need for protecting our environment has increased day by day. Therefore, there is a dire need to remove these organic pollutants from water.

Nowadays, a lot of work is done on photocatalysis because of various environmental problems by using the solar energy source (sunlight). BiFeO_3 (BFO) is a multiferroic material and a good catalyst for photocatalytic activity. The doping of Gadolinium (Gd) and Tin (Sn) into BFO sample ($\text{Bi}_{1-x}\text{Gd}_x\text{Fe}_{1-y}\text{Sn}_y$; BGFSO) also enhanced its catalytic properties. Our research work comprises of the BFO/MXene and BGFSO/MXene nanohybrid samples. MXene are a class of 2D materials having layers of Transition metals like Titanium and layers of Carbon and Nitrogen having a Functional group of OH^- , O^- and F^- attached on its surface. The hybrid of BFO/MXene and ($\text{Bi}_{1-x}\text{Gd}_x\text{Fe}_{1-y}\text{Sn}_y$; BGFSO)/MXene were fabricated by co-precipitation method. The prepared hybrid samples were characterized by different characterization tools like X-Ray diffraction (XRD), Scanning electron microscope (SEM), X-Ray photoelectron spectroscopy (XPS), Photoluminescence spectra (PL) and UV-visible spectra. XRD was used for investigating the phase structure of the prepared hybrid sample. SEM was used for the study of surface morphology of prepared hybrid. XPS was used for the confirmation of elements present in a hybrid sample. PL was used for study the electron-hole recombination rate. Band gap and absorbance spectra were obtained from UV-visible spectra. From the photocatalytic results, it was observed that the BFO/MXene hybrid sample degraded the 100% acetophenone from a catalytic solution. Whereas the ($\text{Bi}_{0.90}\text{Gd}_{0.10}\text{Fe}_{0.95}\text{Sn}_{0.05}$; BGFO-5Sn)/MXene shows the 38% degradation of Congo red dye, ($\text{Bi}_{0.90}\text{Gd}_{0.10}\text{Fe}_{0.90}\text{Sn}_{0.10}$; BGFO-10Sn)/MXene and ($\text{Bi}_{0.90}\text{Gd}_{0.10}\text{Fe}_{0.85}\text{Sn}_{0.15}$; BGFO-15Sn)/MXene shows the 18% degradation and ($\text{Bi}_{0.90}\text{Gd}_{0.10}\text{Fe}_{0.80}\text{Sn}_{0.20}$; BGFO-20Sn)/MXene hybrid sample shows the 100% degradation of Congo red from catalytic solution only in 120 min, this shows that pure BFO/MXene and ($\text{Bi}_{1-x}\text{Gd}_x\text{Fe}_{1-y}\text{Sn}_y$; BGFSO) /MXene hybrid sample are good candidates due to its highest dye degradation efficiency.

Thesis

The layout of this thesis is as follows:

Chapter 1

In this chapter, the general concept of Nanoscience, nanomaterials are presented. The introduction of Bismuth Ferrite (BFO) is also explained.

Chapter 2

This chapter includes the literature survey based on Bismuth Ferrite (BFO) hybrid with 2D materials.

Chapter 3

The third chapter includes synthesis and characterization of hybrid of BFO/MXene and BGFSO/MXene.

Chapter 4

The fourth chapter contains the results and discussions of BFO/MXene.

Chapter 5

The fifth chapter contains the results of BGFSO/MXene.

CHAPTER 1: Introduction

1.1. Introduction to Nanotechnology

The study of different materials at the atomic, molecular and nanoscale level are the base of Nanotechnology. The nanometer scale ranges from 0.1 to 100 nm. One nanometer is one billionth of a meter (10^{-9} m). Therefore, Nanoscience and nanotechnology always deal with objects of 1 nm in size. The material at nanoscale has optical, electrical and mechanical properties which are different from the material at a macro scale. The difference in properties at nanoscale mainly includes the large surface area, large surface to volume ratio and enhanced quantum confinement effects [1].

1.2. History of Nanoscience and its Technology

Nanotechnology is around us in nature and is found in objects having nanometer regime. The Richard Feynman gives the concept of nanotechnology in 1959 “There is a plenty of space at the bottom” [2, 3].

In 1974, the idea of nanotechnology was developed into a scientific world by N. Taniguchi at the international scientific conference held in Tokyo. The main idea behind it to introduce the processing of materials with nanometer range and the formation of nanosized mechanisms. In 1986, the E. Drexler put forward the idea of nanotechnology by publishing his book “Vehicles of Creation, the arrival of nanotechnology era” [4, 5].

In the middle of 1980s and the early of 1990s, a large number of discoveries occurred, and it has an essential impact on the development of nanotechnology.

In 1991, the program of National Scientific Fund based on nanotechnology started in the USA.

During 1992-1998 the scientific experts in USA organized the session on Nanoscience, nanotechnology and nanoengineering. The main theme of organizing this session was to enable us to create new materials having nanometer regime in the future.

In 2000, after the USA the Japanese also put forward his ideas towards the nanotechnology and its further development.

From 2001 to onwards a lot of research has been done on nanotechnology and on its various applications [6, 7].

1.2.1. Applications of Nanotechnology

The history of nanotechnology based on integrated chips. In 1947 the first transistor of macro size was invented. In 2002 the nano size transistor having the dimensions of 90 nm was developed. But at the end of 2009, a single transistor having dimensions of 45 nm was achieved. In 1988 Giant Magnetoresistance technology (GMR) also considered the major application of nanotechnology due to its diversity in various fields. In GMR the electrical resistance of different materials containing magnetic and nonmagnetic layers of various metals can change by applying a large amount of magnetic field. The use of GMR in various data storage devices like MRAM is a great improvement in nanotechnology [8].

1.2.2. Nanomaterials

The materials having the dimensions in the nanometer range 0.1-100 nm are known as nanomaterials. The enhanced and unique optical, magnetic, electrical, chemical and physical properties of nanomaterials make them useful than that of bulk materials. Due to these properties, the nanomaterials have great potential impacts on data storage devices, electronics, energy, biomedicine, catalytic and water splitting applications [9].

1.2.2. Types of Nanomaterials

The nanomaterials can be in single or agglomerated form having irregular, spherical and tabular shapes [10]. On the basis of dimension, nanomaterials are of different types like

- Zero-Dimensional
- One Dimensional
- Two Dimensional
- Three Dimensional

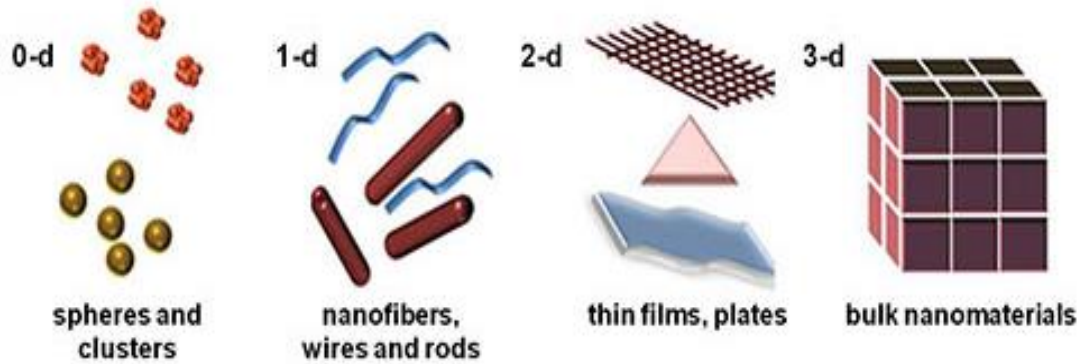


Figure 1.1: Classification of Nanomaterials [11].

1.2.3.1. Zero-Dimensional (0-D)

A material having nano regime in all the three possible directions are known as zero-dimensional material. Nanoshells and quantum dots are the examples of Zero-dimensional (0-D) nanomaterial [11].

1.2.3.2. One dimensional (1-D)

A material has two of its three dimensions are in nanometer range and in one-dimension electron are free to move are known as one dimensional (1-D) nanomaterial. Nanowires, nanorods, and nanotubes are the examples of one dimensional (1-D) nanomaterial. The lengths of one-dimensional material are several micrometers, but the diameter is of few nanometers [11].

1.2.3.3. Two dimensional (2-D)

A material having one of its three dimensions is in nanoscale range is known as two dimensional (2-D) nanomaterials. Nanofilms, nanosheets or nano-walls are the examples of two dimensional (2-D) materials [11].

1.2.3.4. Three Dimensional (3-D)

A material having all three dimensions are in microscale range is known as three dimensional (3-D) nanomaterials. These materials are also considered as bulk materials. Nanotubes, nanowires or nanostructures are the examples of three dimensional (3-D) nanomaterials [11].

1.3. Properties of Bulk and Nanomaterials

Bulk materials are always studied on the basis of their physical properties like their boiling point, melting point, bulk density, and conductivities etc. For the nanomaterials the physical properties are of great interest due to its large surface area and small size that enhances its surface reactivity and important for its optical emission properties by tuning its band gap through doping. Due to the optical emission property nanomaterials have various applications like optical sensors [12], biomedical field [13], and laser and energy storage system [14, 15].

1.4. Multiferroic Materials

Multiferroic materials are those which simultaneously contain ferromagnetic order as well as ferroelectric order [16]. All multiferroic materials exhibit the perovskite structure. Bismuth ferrite (BiFeO_3) and Barium ferrite (BaFeO_3) are the best examples of multiferroic materials due to its magnetic behavior and the variation in magnetic moments induced the electric polarization in the structure [17, 18, 19].

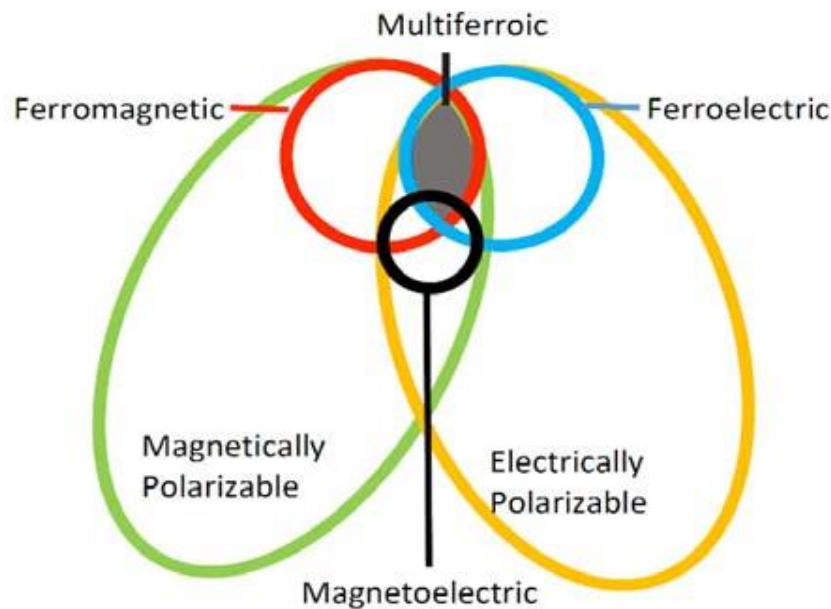


Figure 1.2: Multiferroic property

1.5. Single Phase Multiferroic Material

1.5.1 Bismuth Ferrite

Amongst the large family of multiferroic materials, Bismuth ferrite (BiFeO_3) is the most studied multiferroic material with the perovskite structure. The simplicity of crystal structure and a variation in compositions makes the perovskite structures important for the fabrication of numerous materials [20, 21].

1.5.2 Crystal Structure

All perovskite structures have a general formula (ABO_3), where A and B are cations and O is the anion located in the origin of the lattice. In BiFeO_3 , Bismuth atoms are located at the octahedral sites, iron atoms present at B sites surrounded by Oxygen atoms present in all six faces and form FeO_6 Octahedral. At room temperature, the bismuth ferrite has rhombohedral distorted perovskite structure with space group $R3c$ [22]. The rhombohedral structure transforms into the orthorhombic structure when metals are doped into bismuth ferrite nanoparticles [23]. BiFeO_3 , BiMnO_3 , BaFeO_3 , TbMnO_3 etc are the important multiferroic materials belong to the perovskite family [24, 25].

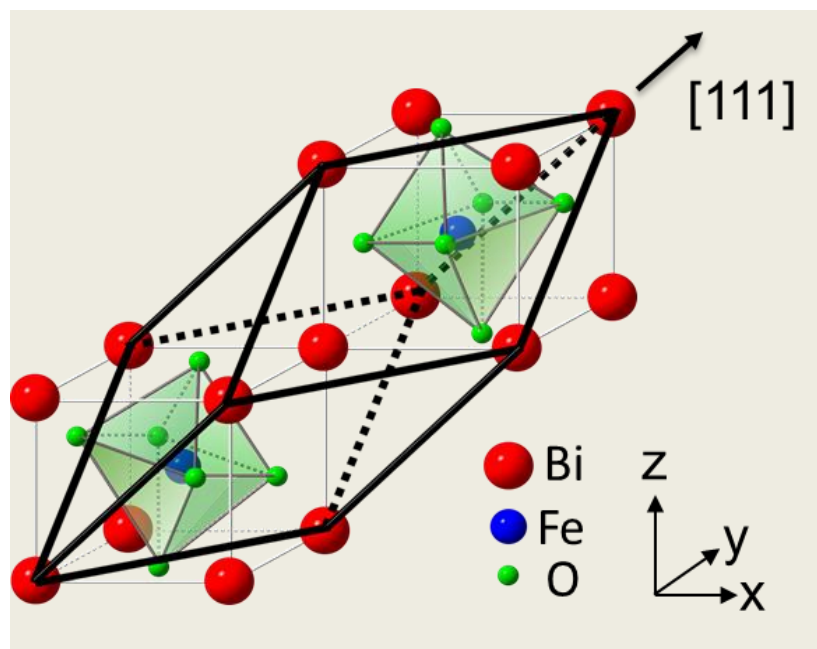


Figure 1.3: Structure of BFO [24]

1.5.3. Drawbacks of BiFeO₃

Although the Bismuth ferrite has a good ferroelectric and ferromagnetic properties along with that, it has some drawbacks like the formation of an impurity phase, such as Bi₂Fe₄O₉, Bi₂₄Fe₂O₃₉, Bi₃₆Fe₂O₅₇, or (Bi₂₅FeO₄₀) etc. These phases arise due to the high electronegativity of Oxygen atom present in a compound as well as the volatile nature of bismuth at high temperature [26- 28]. These impurity peaks do not affect the structure and bonding of atoms of a material but somehow affect the electrical, magnetic and the optical properties of BiFeO₃ [29].

1.6. Daily applications of Nanomaterials

Nanomaterials have a large number of applications in this advanced world on the basis of extraordinary and beneficial properties. In this modern era the various applications include biosensors [30], fuel cells [31], medical field [32], electronics [33], agriculture field [34] etc.

All the multiferroic materials possess various applications in the field of electronics like data storage devices, spintronic devices, and include energy devices etc. [35]. With the doping of rare earth elements in Bismuth Ferrite (BFO) the photocatalytic applications and bacterial activity can be improved.

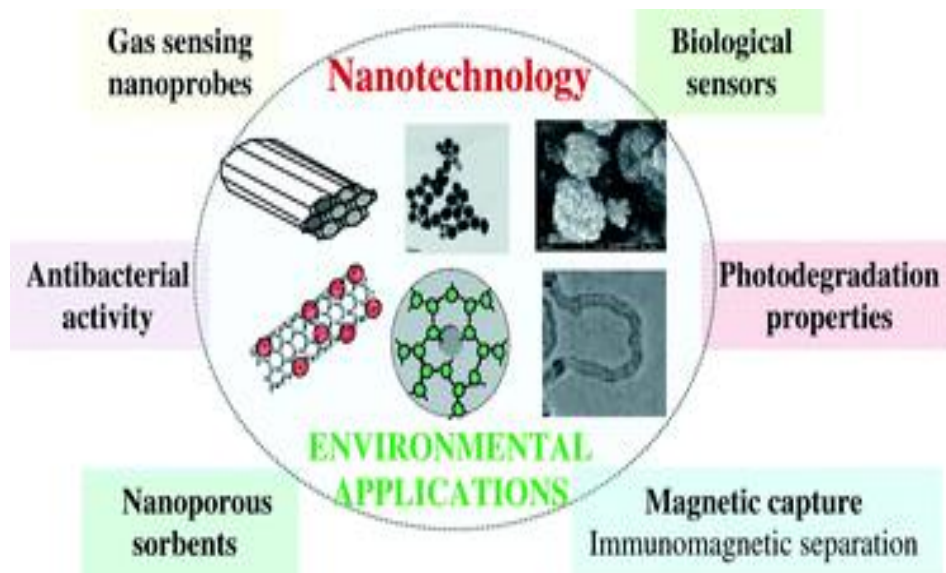


Figure 1.4: Environmental Applications of Nano materials.

1.6.1. Solar Cells

Now a day's Nanomaterials and their hybrid are used in the production of solar cells based on the variation in size and its efficiency. Photovoltaic is the most common type of solar cells that convert solar light into electricity. Semiconductor materials are used in the production of solar cells because of its tunable band gap that enhances its efficiency and stability than that of bulk materials.



Figure 1.5: Solar Cells

1.6.2. Nano- Electronic Devices

Nanotechnology brings a great revolution in the field of electronics. In the field of electronics, the contribution of nanomaterials is not limited, but it increases day by day by reducing the size of devices like capacitors and transistors etc. So, Nanomaterials and nanoscience are playing an important role in the diverse field of electronics, such as in data storage devices, ultra-capacitor, and supercapacitor etc.

- **Data Storage Devices**

The data storage devices rely on the production of transistors. By reducing the size of transistors, the data storage capability can be enhanced. All such devices based upon the concept of spintronics. Giant Magneto Resistance (GMR) and Tunneling Magneto Resistance (TMR) are the two effects that led to increasing the nonvolatile data storage capacity of hard disks through ferromagnetism.

- **Ultracapacitor or Supercapacitor**

Now a day's nanocomposites of Graphene oxide, reduced graphene oxide and MXene sheets have used in various applications of energy storage devices like ultracapacitors or Supercapacitor.

1.6.3. Catalytic Property and Environmental control

Nanomaterials are also termed as nanocatalysts due to its large surface to volume ratio and having a large surface area. This property of nanomaterials increases the reaction rate. Metal oxides are mostly used as a photocatalyst material i.e. TiO_2 , BFO, and ZnO etc. The efficiency of the photocatalyst can be enhanced by using hybrid samples i.e the hybrid of BFO/GO and BFO/MXene etc that enhances the surface area of the nanoparticles because of the presence of 2D sheets.

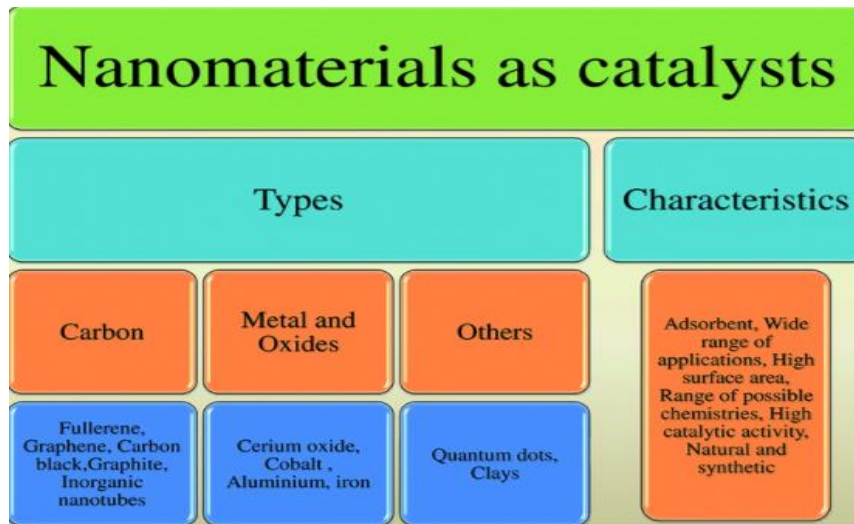


Figure 1.6: Nanomaterials as catalysts

1.6.4. Sensing Devices

Nanomaterials also used in various sensing devices like

- Magnetic sensors
- Temperature and in different pressure sensors
- PH sensors
- Molecules detecting sensors in the biology field

1.6.5. Microelectronic industry

In the industry of microelectronics, the devices having nanometer range play an important role due to its small size and large surface area. Mostly capacitors and transistors are included in the microelectronic industry.

1.6.6. Display Screens (TV)

Now a day nanomaterial brings revolution in various display screens. Mostly the Phosphorous material is used. When the electron beam interacts with Phosphorous screen then it lights up. In order to obtain the better resolution, the pixel size must be reduced. And it is possible only if we used nanocrystalline materials like zinc sulphide and cadmium sulphide. The zinc sulphide and cadmium sulphide are the good Nanocrystals.

1.6.7. Space Exploration

The carbon nanomaterials are used in space shuttles because of its light weight and greater strength. By using the different hybrid structures the efficiency and strength of spaceships can be increased.

CHAPTER: 2 Literature Review

Our research work is comprised of hybrid system that was prepared using Gadolinium (Gd^{3+}) and Tin doped (Sn^{4+}) Bismuth ferrite and undoped Bismuth ferrite with 2D MXene sheets with their enhanced degradation properties for Congo red dye as well as Acetophenone (colorless compound). A lot of work has been done on dye degradation using nanoparticles, using 2D sheets like Graphene and Reduced graphene oxide and their hybrid structures etc. Now a day's scientist is working on 2D MXene sheets for its multidimensional properties and its various hybrid structures that are also under studies.

Shun Li et al in 2009 prepared the BFO nanostructures using the hydrothermal technique. From the characterization techniques, it was observed that the BFO nanostructures are of small in size and has an average diameter of 5 nm. The small size of particles enhances the surface area. Hence it was helpful for improving the dye degradation reaction. The band gap of BFO particles was also shown to be direct band gap so it enhances the electron and hole recombination time. The low recombination of charge carriers hinders the fast degradation of dye molecules. In view of all these factors, the maximum degradation of Congo red takes place in BFO nanostructures. 95% of dye degraded in only 2 hours and shows that the BFO are a good catalyst for other dye degradations [36].

In 2010, the Renqing Guo et al reported the synthesis of doped Bismuth ferrite nanoparticles using Gadolinium (Gd^{3+}) as a dopant atom $Bi_{1-x}Gd_xFeO_3$ ($BGFO_x$, $x = 0, 0.05, 0.1, \text{ and } 0.15$) by a sol-gel method for testing the Rhoda mine-B (RhB) degradation from a catalytic solution ($BGFO$). X-Ray diffraction (XRD) shows the crystalline nature of the prepared sample. SEM used for the study the surface morphology of the sample. With the increase of doping concentration average particle size going to decrease and enhances its surface area. The greater surface area allows more adsorption of dye molecules over the catalytic surface. So, 5% degradation of RhB was observed under dark experiment whereas 94% degradation of RhB occurred using $BGFO_{x=0.15}$ in the presence of visible light [37].

Jian He et al in 2013 give a report on the synthesis of BFO nanoparticles by a simple and easy sol-gel method. Bismuth ferrite (BFO) is a good multiferroic material. Different fabrications used for the confirmation of prepared nanoparticles like XRD, SEM, Raman measurement and UV-visible spectroscopy. The BFO nanoparticles were used for the examination of dye degradation activity. The size of nanoparticles effects the functionality of photocatalytic activity. In the present reported work, the Rhodamine B dye degraded from a solution. 15% degradation of Rhodamine B was reported in 180 minutes using visible light [38].

Sakar Mohan et al in 2014 have also fabricated the Gadolinium (Gd^{3+}) doped Bismuth ferrite (BFO) nanoparticles by simple sol-gel method. From XRD it was clear that the particle size going to decrease with the increase of doping concentration of Gadolinium (Gd^{3+}). A SEM result shows that upon doping the shape of BFO nanoparticles changes for irregular to spherical shape. Gadolinium being a magnetic material enhances the magnetic properties of BFO nanoparticles. The prepared nanoparticles used for degradation of Methylene blue (MB). It was observed that by increasing the doping concentration of Gadolinium the bandgap going to be reduced from 2.38 e.V to 2.29 e.V. The tuning of bandgap increases the dye degradation process so using visible light the 90% degradation of Methylene blue (MB) takes place in 4 hours [39].

Syed Irfan et al in 2017 studied the Samarium (Sa) and Manganese (Mn) doped Bismuth Ferrite (BFO) with different concentrations of Manganese (Mn) having doping formula of $Bi_{1-x}Sm_xFe_{1-y}Mn_yO_3$ (BSFMO, $x=0.0, 0.05$; $y=0.0, 0.05, 0.10, 0.15, 0.20, 0.25$). The BSFMO nanoparticles were synthesized by sol-gel technique. Different characterizations were performed for study the structure and morphology of nanoparticles like XRD, SEM etc. By increasing the doping concentration of Sm and Mn the crystallite size decreases from 57.3 nm to 17.2 nm. The band gap tuned from 2.08 e.V to 1.45 e.V because of the formation of forbidden energy levels upon the incorporation of dopant. SEM results reveal the irregular shape of doped nanoparticles. The prepared nanoparticles used for testing the organic dyes i.e. Methylene blue, Methyl violet and Congo red. Using visible light 65% of Methylene blue, 64% of Methyl violet and 97% of Congo red degradation took place from a dye and catalytic solution within 2 hours [40].

Syed Irfan et al in 2017 also synthesized the Tin (Sn^{4+}) and Gadolinium (Gd^{3+}) doped Bismuth ferrite (BFO) nanoparticles with different concentrations of Tin (Sn^{4+}) having concentration formula of $\text{Bi}_{1-x}\text{Gd}_x\text{Fe}_{1-y}\text{Sn}_y\text{O}_3$ (BGFSO; $x = 0.0, 0.01$; $y = 0.0, 0.05, 0.10$). The BGFSO nanoparticles prepared by sol-gel method and used for checking the degradation activity of Congo red, Methylene blue and Methyl violet. From XRD results the confirmation of crystalline nanoparticles was predicated. The average particle size calculated using Debye Scherrer's equation was found to be 60 nm, 18 nm, and 22 nm. SEM results show the irregular shape of particles. The band gap calculated using the Tauc plot was estimated to be from 2.10 e.V to 2.03 e.V. The doped nanoparticles behave as a catalyst for the degradation of dye molecules from a solution. 44% degradation of Congo red, 40% Methylene blue and 19% degradation of Methyl violet were takes place using BFO nanoparticles, whereas a large amount of dye degradation (95% Congo red, 95% Methylene blue and 64% Methyl violet) takes place using BGFO-5Sn nanoparticles [41].

Syed Irfan in 2017 et al have also reported on Lanthanum (La^{3+}) and Selenium (Se^{4+}) co-doped Bismuth ferrite (BFO) nanostructures. The simple sol-gel technique was used for the fabrication of co-doped BFO structures. Different characterization was performed for the confirmation of prepared nanostructures, but the important one was the UV-visible spectrometer used for checking the absorbance and degradation of Congo red and Acetophenone from dye solution. 82% of Congo red and acetophenone degradation takes place in 50 minutes under visible light. Although it is very difficult for acetophenone to degrade because of its stable structure the good photocatalytic results were estimated to be because of low crystallite size (123 nm to 80 nm), large surface area, tuneable bandgap and low electron-hole recombination [42].

Christelle pau ping pong et al in 2015 checked the degradation of Remazol Black B (RB5) using RGO. RGO nanoparticles were fabricated using a chemical reduction method of GO and GO was prepared by Hummer method. The nanoparticles of RGO were confirmed by different characterization techniques i.e. X-Ray diffraction (XRD), Scanning electron microscope (SEM), Raman and UV-visible spectrophotometry. XRD results show the peak at 24.1° and this peak corresponds to the RGO peak. It was observed that 56% of RB5 degraded from RGO solution

under visible light in only 60 minutes. This confirms that RGO also behaves as a catalyst for photocatalytic activity [43].

Yongye Liang et al studied in 2010 the TiO₂/GO hybrid sample that was synthesized by hydrothermal method. The prepared hybrid sample was used for dye degradation activity of Rhodamine B. The confirmation of the prepared hybrid was estimated from XRD and SEM results. The hybrid of TiO₂/GO plays an important role in the photocatalytic activity. The 100% degradation of Rhodamine B reported in only 20 minutes under ultraviolet (UV) light [44].

Yongsheng Fu et al in 2012 prepared the Copper Ferrite/Graphene Oxide (CuFe₂O₄/GO) hybrid by two step hydrothermal method. The copper ferrite is a good magnetic material as well as a good photocatalyst. The combination of copper ferrite with graphene oxide makes a dramatic enhancement in the properties of copper ferrite material. The hybrid sample was used for testing the degradation of Methylene blue (MB) used as a pollutant in a catalytic solution. The prepared solution was irradiated with visible light. It was observed that 100% degradation of Methylene blue (MB) takes place in 4 hours using a different concentration of Graphene in (CuFe₂O₄/GO) hybrid sample [45].

Zhuoxuan Li et al in 2014 fabricated the BFO/GO hybrid using hydrothermal treatment for testing the degradation of Congo red under visible light irradiation. The structure and morphology of the prepared hybrid were determined from XRD and SEM. The crystalline nature of BFO/GO hybrid confirmed from XRD with an average crystallite size of 100 nm. SEM results show that the BFO nanoparticles attached on GO sheets. The tuning of bandgap was from 1.78 e.V to 2.24 e.V also helpful for improving the photocatalytic activity. The formation of chemical bonding between the elements of BFO nanoparticles and graphene oxide sheets (GO) was confirmed from XPS. The hybrid of BFO/GO was used for study the photocatalytic activity. The hybrid used for checking the degradation of Congo red dye from catalytic solution. It was observed that 48% degradation of Congo red reported under visible light in only 120 minutes. The obtained result was very close to the degradation result of Congo red using pure BFO nanoparticles [46].

J. F. Dai et al in 2013 also fabricated the BFO/GO hybrid structure by a simple sol-gel method. The photocatalytic degradation activity of Methyl Orange (MO) dye was reported using the visible light source. It was observed that 55% degradation of dye from a hybrid solution in 5 hours takes place. The result of dye degradation in case of BFO/GO was highly improved and better than the pure BFO nanoparticles used for degradation of Methylene Orange (MO) [47].

Huajun Sun et al in 2014 synthesized the $\text{Bi}_2\text{Fe}_4\text{O}_9/\text{RGO}$ hybrid by hydrothermal treatment. Different characterization was performed for the confirmation of hybrid i.e. XRD, SEM, Raman and UV- visible etc. The prepared hybrid used for Methyl violet degradation from a catalytic solution. 95% Methyl violet degradation was reported using visible light in 180 minutes. This indicates the enhanced catalytic properties of $\text{Bi}_2\text{Fe}_4\text{O}_9$ with the incorporation of RGO [48].

Aiwu Sun et al in 2013 fabricated the hybrid of $\text{Bi}_{25}\text{FeO}_{40}/\text{GO}$ by a single step hydrothermal method. The confirmation of prepared $\text{Bi}_{25}\text{FeO}_{40}/\text{GO}$ hybrid was analyzed by various characterization tools (XRD, SEM, EDX, XPS and UV-visible etc). The prepared hybrid sample was used for testing the photocatalytic activity of Methylene blue (MB) under visible light irradiation. It was noted that 65% of Methylene blue was degraded from a solution using $\text{Bi}_{25}\text{FeO}_{40}/\text{GO}$ catalyst in only 180 minutes [49].

Xingang Zhang et al in 2015 investigate the novel metals hybrid i.e. Ag/BFO and Au/BFO that was synthesized by sol-gel method. The confirmation of prepared hybrid samples was determined by the XRD and SEM techniques. The obtaining hybrid sample was highly crystalline in nature. Ag/BFO and Au/BFO hybrid samples were used for the degradation of RhB under visible light from an aqueous solution. The Ag/BFO sample degraded the 32% of RhB in 7 hours under visible light whereas the Au/BFO degraded the 15% RhB in 7 hours [50].

Huidan Lu et al in 2015 studied the nanocomposites of Ag/BFO fabricated by a sol-gel process. The Ag/BFO nanocomposite characterized by different characterizations tools i.e. XRD, SEM, TEM, UV-visible spectroscopy. The XRD results show the highly crystalline nature of nanocomposite with a particle size of 20 nm to 50 nm. From SEM results it was clear that Ag particles loaded on BFO nanoparticles. The loading of Ag nanoparticles with BFO nanoparticles

enhance the catalytic properties of a nanocomposite. The nanocomposites used for the photocatalytic activity of Methyl Orange (MO). The 9% Methyl Orange (MO) degraded from the catalytic solution under dark experiment whereas 85% of MO degraded with visible light in only 90 minutes. The degradation results indicate that Ag/BFO nanocomposite is a good catalyst than that of pure BFO because of its highly enhanced magnetic properties, large surface area and low band gap [51].

M. Humayun in 2016 reported the TiO_2/BFO nanocomposite synthesized by wet chemical process. The nanocomposites play an important role in enhancing the separation of charge carriers and promote the dye degradation activity. The prepared nanocomposite as a photocatalyst used for the degradation of acetaldehyde and phenol and it was observed that the 70% degradation of acetaldehyde and phenol in only 1 hour [52].

O. Mashtalir et al in 2014 work on the 2D MXene sheets also known as transition metal carbides and nitrides with the different functional group attached on its surface. It was observed that MXene sheets undergo high adsorption and degradation activity, so it is also a good catalyst for photocatalytic activity because of its large surface area. It was used for the degradation of Methylene blue (MB). It degraded the 62% Methylene blue (MB) using visible light in 6 hours [53].

Chao Peng et al in 2016 synthesized the $\text{TiO}_2/\text{Ti}_3\text{C}_2$ hybrid structure by using the approach of the hydrothermal method. The large surface area and porous nature of Ti_3C_2 sheets with TiO_2 help out in order to enhance the photocatalytic activity. The prepared hybrid structures used for degrading the Methyl Orange (MO) dye from a catalytic solution. It was noted that 100% degradation of Methyl Orange (MO) observed in 50 minutes using ultraviolet light. The high photocatalytic activity was estimated to be because of low electron-hole recombination due to the incorporation of MXene sheets as well as large surface area [54].

Yupeng Gao et al in 2015 also synthesized the hybrid of $\text{TiO}_2/\text{Ti}_3\text{C}_2$ by hydrothermal method and reported the photocatalytic activity. The confirmation of the prepared hybrid was illustrated from XRD and SEM results. From XRD results the pure crystalline nature was observed whereas the

SEM results show the presence of TiO₂ nanoparticles on MXene sheets. MXene sheets having large surface area play an important role in the adsorption of dye molecules over it. The fabricated hybrid sample was used for testing the photocatalytic activity of Methyl Orange (MO) in ultraviolet light. It was observed that 98% Methyl orange degraded in only 30 minutes [55].

CHAPTER: 3 Synthesis and Characterization Tools

Apparatus and synthesis procedure

3.1 Apparatus used

The apparatus used during chemical etching of MAX powder as well as the synthesis of doped and undoped Bismuth Ferrite (BFO) nanoparticles and their hybrid formation with MXene sheets are the following;

- Weight balance
- Hotplate
- Sonicator
- Vacuum drying oven
- Petri dish
- Beakers
- Glass rod stirrer
- Whatman filter paper (0.2 μ m)

3.2 Chemicals

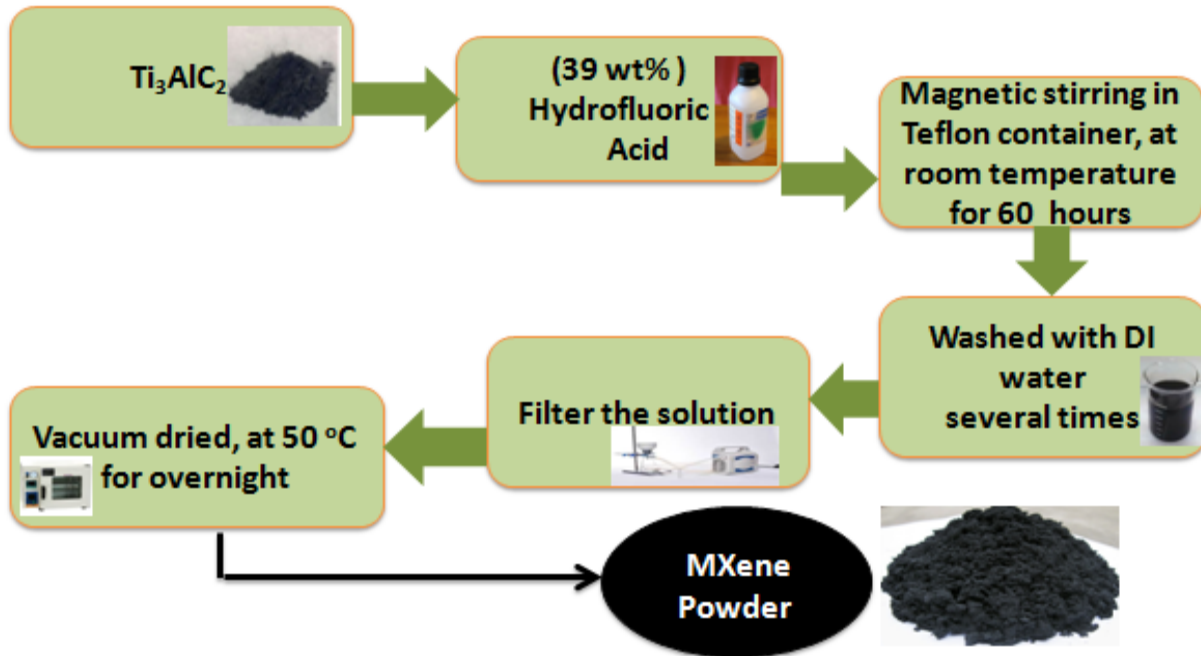
Bismuth nitrate pentahydrate ($\text{Bi}(\text{NO}_3)_3 \cdot 5\text{H}_2\text{O}$), Iron nitrate ($\text{Fe}(\text{NO}_3)_3 \cdot 9\text{H}_2\text{O}$), Gadolinium nitrate, Tin powder, Ethylene glycol ($\text{C}_2\text{H}_6\text{O}_2$), Acetic acid ($\text{C}_2\text{H}_4\text{O}_2$), Hydrofluoric Acid (39 wt%), Ti_3AlC_2 (MAX Powder), Deionized water, Ethanol, Distilled water, Etched MXene powder.

3.3 Synthesis route of 2D MXene sheets

The MXene sheets were prepared by chemical etching of MAX powder (Ti_3AlC_2). Take 10 gram of MAX powder and dissolved it in 200 ml of 39% concentrated Hydrofluoric acid (HF) acid in a Teflon bottle. A Teflon bottle was placed on a magnetic hot plate for the magnetic stirring of about 36 hours at room temperature. After 36 hours the hot plate was turned off for 10 hours and further stirring for 14 hours. The stirred solution was put into a beaker and washed it several times with de-ionized water (DI) and check out the PH of the solution after each washing. After

several items of washing the powder solution was filtered out and dried it in a drying oven for 24 hours at 50 °C, finally, the drying powder was the etched MXene [54, 55].

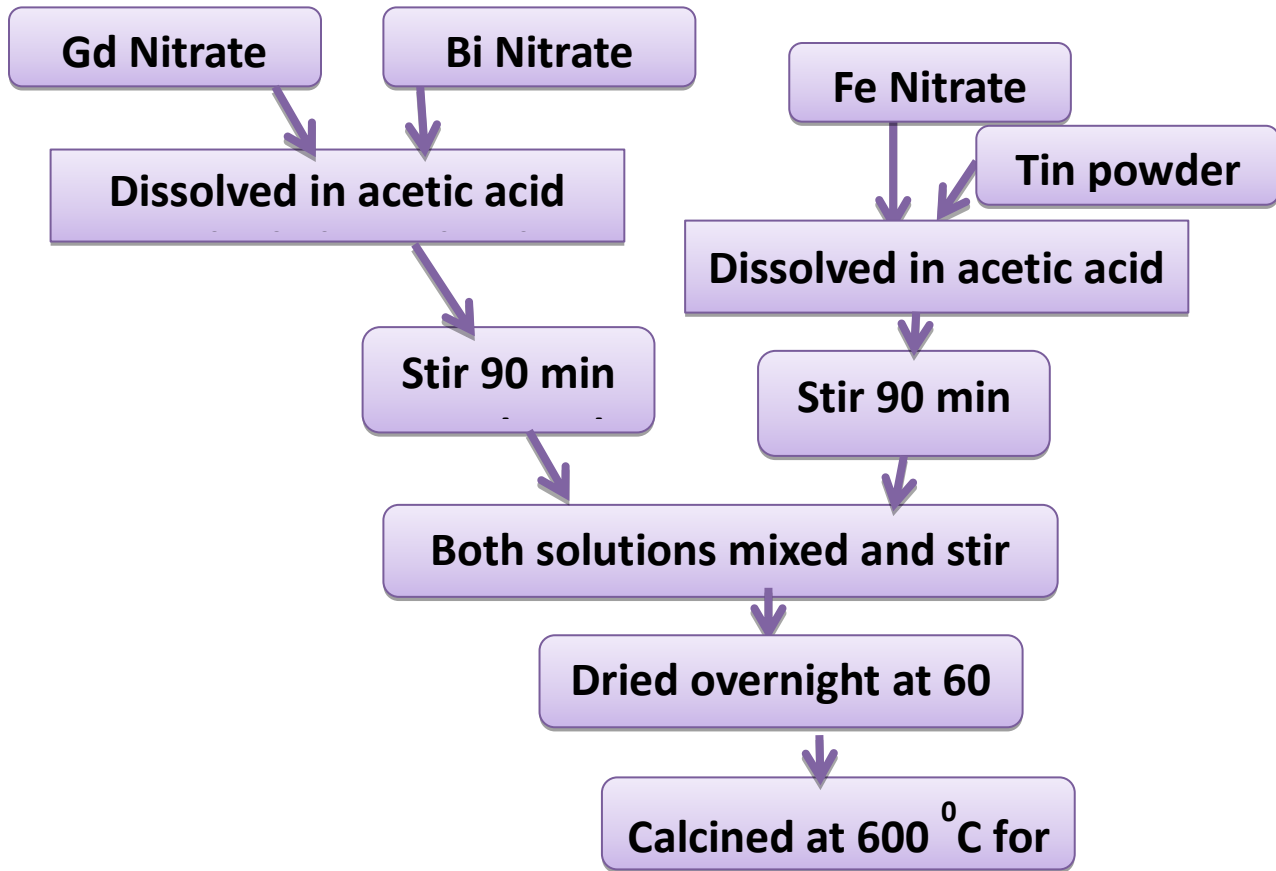
MAX Etching Flow Chart:



3.4 Synthesis of Gadolinium and Tin doped BFO nanoparticles

The Gadolinium (Gd^{3+}) and Tin (Sn^{4+}) doped BFO nanoparticles were synthesized by sol-gel method. The dopant formula for Gd and Sn-doped BFO are $Bi_{1-x}Gd_xFe_{1-y}Sn_yO_3$ ($x=0.10$; $y=0, 0.5, 0.10, 0.20$). The Bismuth nitrate and Gadolinium nitrate powder were added into the solution of acetic acid and ethylene glycol having a molar ratio of 1:1. The prepared solution was stirred using a magnetic hot plate for 2 hours at the temperature of 60 °C. Meanwhile, the Iron nitrate and Tin powder were mixed in an acetic acid and ethylene glycol solution and stir it under the same conditions used for Bismuth ferrite and Gadolinium. Then both prepared solutions mixed together and again undergo the stirring for at least 2 hours at 40 °C. Finally, a reddish-brown solution was obtained having precipitates at the bottom of the beaker. The solution was washed with deionized water and after that dried it in a drying oven for 24 overnight at 60 °C and calcined it 3 hours at 600 °C. The final product was the doped BFO powder [37, 39].

Gd, Sn-doped BFO Synthesis Flow Chart:

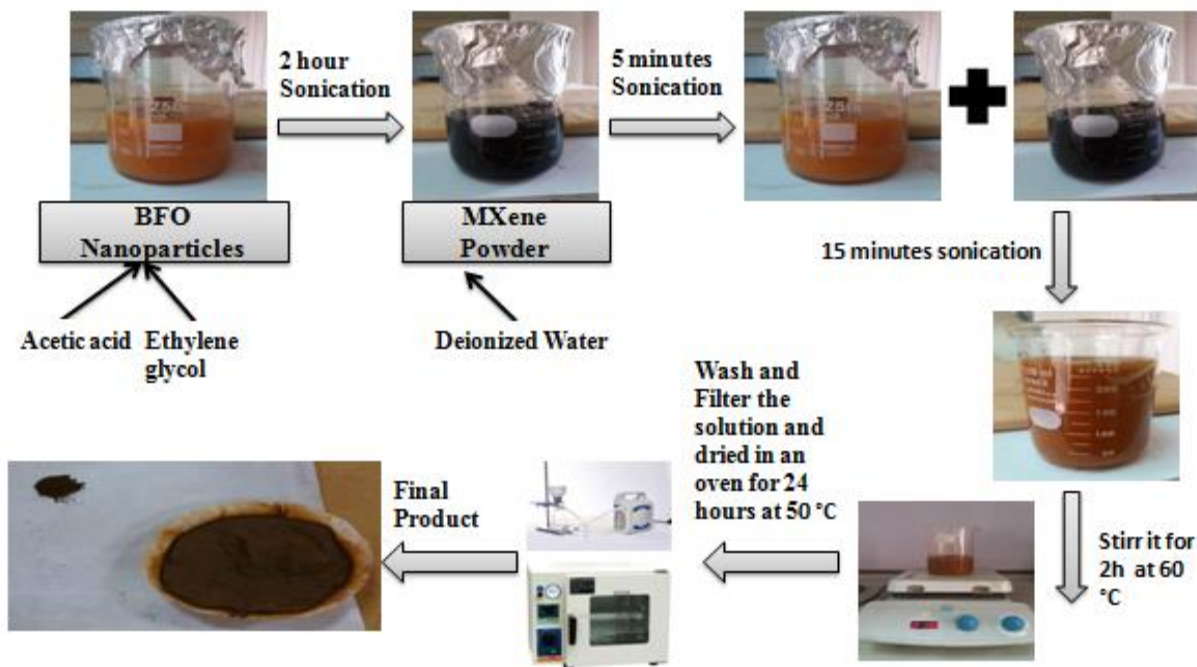


3.5 Synthesis of BFO/MXene hybrid and Gd and Sn-doped BFO (BGFSO/MXene) hybrid

The hybrid of doped and undoped BFO with MXene was synthesized by simple Co-precipitation method. The solution of BFO nanoparticles was prepared in an acetic acid and ethylene glycol that act as a catalyst and solvent respectively. The solution of ethylene glycol and acetic acid were of equal molar concentration (0.01 M). The solution containing BFO nanoparticles were sonicated for 2 hours at 50 °C until a homogeneous solution was obtained. On the other side add required amount of MXene sheets into deionized water and sonicate it for 5 min. After that, both solutions were added together and again sonicate it for 30 min. A gray color solution was obtained after mixing then the solution was stirred magnetically with the help of a magnetic stirrer for 2 hours at 80 °C. Rinse the solution with deionized water and filter it with the help of

vacuum filtration pump. The obtained powder after filtration dried in an oven for 24 hours at 50 °C. Similarly, the other hybrid samples were also prepared by the same technique and process.

Ferrites/MXene Synthesis Flow Chart:



3.6 Characterization Tools

Different characterization tools are used for study the phase identification, surface morphology, elemental and chemical composition, band gap, electron and hole recombination and degradation efficiency of dye from a catalytic solution. Following are the main characterization tools used for measuring the different parameters of prepared hybrid samples.

- X-Ray Diffraction (XRD)
- Scanning electron microscope (SEM)
- UV-vis-spectrometer
- Spectro fluorometer- PL (Photoluminescence spectroscopy)
- X-Ray photoelectron spectroscopy (XPS)
- Photocatalytic measurement

3.6.1 X-Ray Diffraction (XRD)

XRD used for phase identification and structural analysis of various materials. It is a nondestructive technique. This technique also used for the determination of lattice constant, interplanar distance, crystallite size using Scherrer formula, the volume of the unit cell and all other parameters related to the structure of the material.

Basic Principle:

X-Ray diffraction (XRD) works on the principle of Bragg's law. The interaction of a monochromatic radiation with the material produced the constructive interference and satisfied the Bragg's condition

$$n\lambda = 2d\sin\theta \quad (1)$$

Where,

n = positive integer

λ = Wavelength of incident light

d = Interplanar distance

θ = Scattering angle

A sample placed on the specimen and the detector rotated at an angle of 2θ in order to record the diffraction beam scattered at all sides. A peak appeared only when the Bragg's condition is satisfied. From the peaks of the sample, we determined that either the material is crystalline or amorphous.

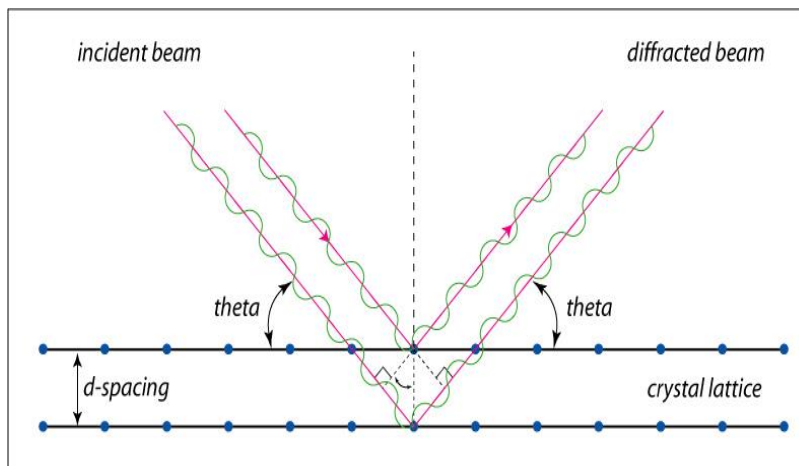


Figure: 3.1 Braggs Law [57, 58]

Experimental Arrangement

The beam of X-Rays is produced when a tungsten filament is heated by applying a voltage. The emitted electrons produced by heating tungsten filament are accelerated towards the anode and after striking with the target metal these electrons have enough energy to knock out the core-shell electrons of the target sample and hence X-Rays are produced. Mostly $\text{CuK}\alpha$ radiations are used for XRD analysis because of its high energy 8048 eV as compare to other radiations i.e. $\text{MgK}\alpha$, $\text{AlK}\alpha$ etc [57, 58].

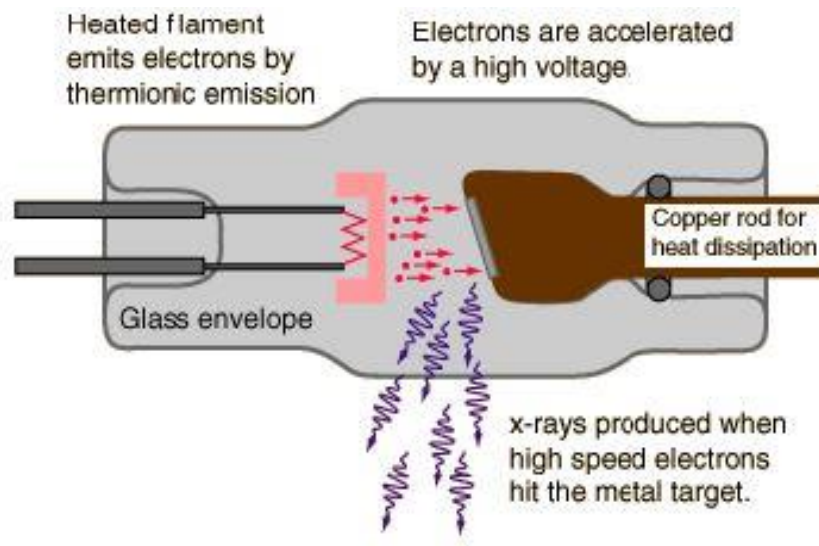


Figure: 3.2 X-Ray Generation phenomena [57]

3.6.2 Scanning Electron Microscope (SEM)

Scanning electron microscope (SEM) is a microscopic technique used for study the surface morphology of the sample. A high electron interacts with a sample placed on the specimen after interaction it gives different signals that are recorded by a detector. The recorded signals help out to study the morphological analysis of the sample. The resolution power of SEM was estimated to be 1 nm [59].

Components of SEM instrument

Following are the components of SEM apparatus

- Electron gun
- Electromagnetic lens

- Magnetic scanning coils
- Sample holder
- Detectors
- Computer

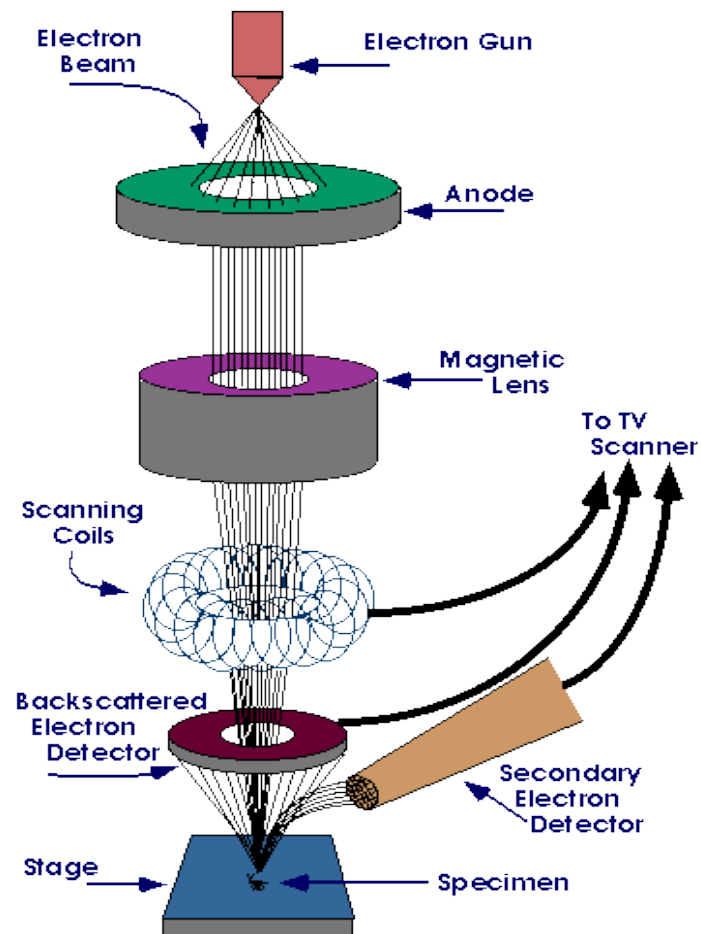


Figure: 3.3 SEM Construction [59]

SEM Working

- In SEM the electron gun is used to produce the beam of electrons and directed it onto the sample.
- The electromagnetic lens used to focus the electron beam onto the target material.
- Scanning coils used to control the beam of an electron by applying a magnetic field with carrying current in the scanning coils that contains solenoids in it.
- A sample is placed on the sample holder having a flat surface.

- In SEM different type of detectors (Secondary and backscattered electron detector) used for detecting the signals generated upon the interaction of electron beam with the sample.
- The detecting signals display on the computer screen.

EDXS (Energy dispersive X-Ray spectrometer)

The EDXS technique is used for the elemental identification of the sample. A SEM instrument attached with EDXS system for performing the material compositional analysis. It is also used for estimating the ratio of elements present in a sample or compound.

3.6.3 UV-vis-spectrometer

It is a technique used for the measurement of electromagnetic radiations absorbed into a material. The range of these radiations according to its energy is Ultraviolet (100 nm-400 nm), Visible (400 nm-700 nm) and infrared lie above 700 nm. The vacuum condition must be achieved for measuring the UV-vis spectrum of the sample.

Principle

It works on the principle of Beer-Lambert law. The Beer-Lambert law states that when a monochromatic light can pass through a solution then the light absorbed into a solution is directly proportional to the concentration of the solution as well as path length of the cuvette.

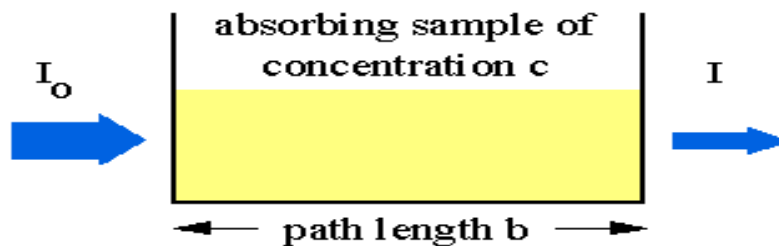


Figure: 3.4 Beer-Lambert Law [60]

Mathematically the Beer-Lambert law states that

$$A = \epsilon c l \quad (2)$$

A= Absorbance of light

ϵ = Absorptivity

C= Concentration of solution

l= Path length of solution

Working and Experimental setup

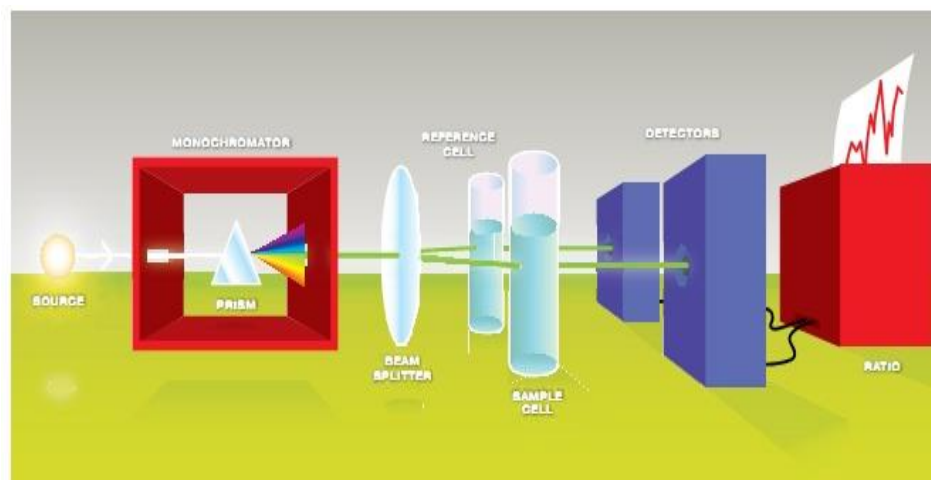


Figure: 3.5 A set up of UV- visible spectroscopy [60]

A monochromatic beam of light focused on a prism that acts as a diffraction grating and allows it to split the beam into different wavelengths of light. The beam splitter also split the beam into two beams. One beam is passing through the sample cell and other beam passing through the reference solution. The intensities of both beams measured by a detector and it confirmed that the light passing through a sample cell has low intensity whereas light passing through a sample solution are of high intensity because of more absorption of light into a solution due to the presence of large no. of molecules in it that absorbed a large amount of light for undergoing the transitions [60, 61].

Bandgap using Tauc plot

The band gap calculated using Tauc plot with the help UV absorbance spectra using the UV-visible spectrometer. The expression for the Tauc plot is as follows [40]:

$$(\alpha h\nu)^n = A (h\nu - E_g) \quad (3)$$

Whereas,

α = Absorbance

h = Planck's constant

A = Proportionality constant

ν = Frequency of vibrations

E_g = Band gap energy

n = Nature of optical transitions

Moreover $n = 2$ for directly allowed transitions and $n = \frac{1}{2}$ for indirect allowed transitions. For direct Band gap, a plotting occurs between $h\nu$ and $(\alpha h\nu)^2$ and a straight line is obtained whereas for the determination of indirect band gap a graph between $h\nu$ and $(\alpha h\nu)^{1/2}$ is plotted. After that, the straight line was extra plotted towards the x-axis and a point at which this line meets with x-axis gives the band gap value [62].

3.6.4 Photoluminescence spectra (PL)

Photoluminescence (PL) spectra are a technique associated with the recombination of electrons and holes.

Principle

Photoluminescence (PL) works on the principle of transition of electrons from the conduction band (CB) to the valence band (VB). When electrons interact with holes then the loss of energy takes place, this loss of energy is in the form of radiations emitted from the surface of the material and generates luminescence. The emitted radiations collected by the detector and it generates Photoluminescence spectra on screen [63].

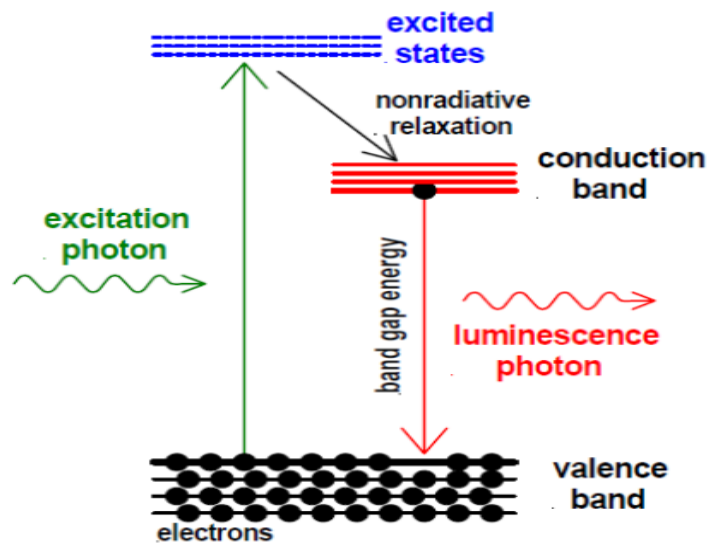


Figure: 3.6 PL Principle [63]

3.6.5 X-Ray photoelectron spectroscopy (XPS)

X-Ray spectroscopy is a nondestructive technique used for study the surface chemistry as well as elemental identification of a material. In XPS the X-Ray photons with an energy of 200-2000 e.V used for the emission of photoelectrons form material surface. The energy of the excited photoelectrons helps in determining the elemental ratio of compound [64].

Principle

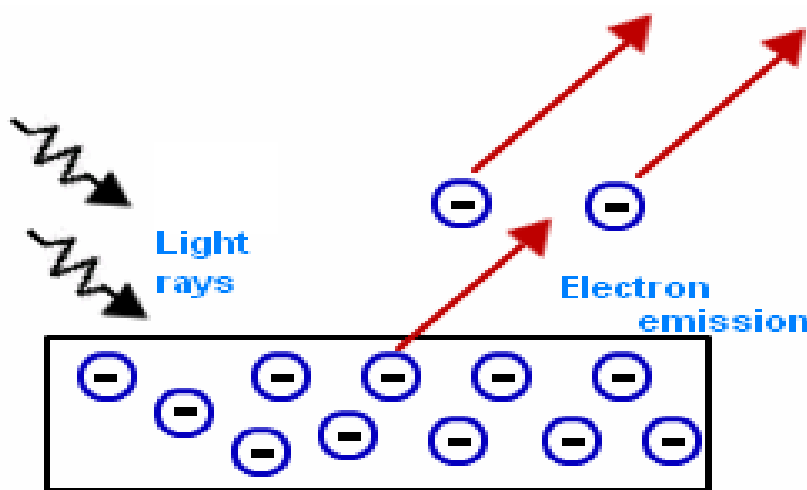


Figure: 3.7 XPS Principle [64]

It works on the principle “Photoelectric effect”. The interaction of light rays with the target material transfer its energy to the electrons of the material and as a result, after getting energy the electrons knock out from material surface and give the information about the binding energy (e.V) as well as the kinetic energy (e.V).

3.6.6 Photocatalytic degradation activity

For the degradation of various organic dyes, a photocatalytic activity was performed using UV-visible spectroscopy. The experimental method used for the photocatalytic activity was based on the catalyst and dye solution. The 100 mg catalyst powder (hybrid sample) was added into 100 ml of the dye solution and stirs it for 10 minutes. After that, the solution was kept in a dark place for checking the degradation of dye under dark effects. Then the light was irradiated on the

solution for speed up the degradation reaction. Different wavelengths of light can be used in reaction i.e. ultraviolet light (100 nm-400 nm) as well as visible light (400 nm-700 nm). In present work a Xenon lamp of 300 W used as a visible light source for generation of charge carriers. Make sure that the distance between the solution and the light generated lamp must be 5 cm for good catalytic results. After 30 minutes a small amount of solution was taken out and centrifuged at speed of 7000 rpm. Characterize the centrifuged sample through UV-visible spectroscopy for checking the dye absorbance and its degradation from a catalytic surface. The Process will be repeated several times until a dye color discharges.

CHAPTER 4 Results and Discussion-I

4.1. Part A: BFO/MXENE Hybrid

4.1.1. X-Ray Diffraction (XRD)

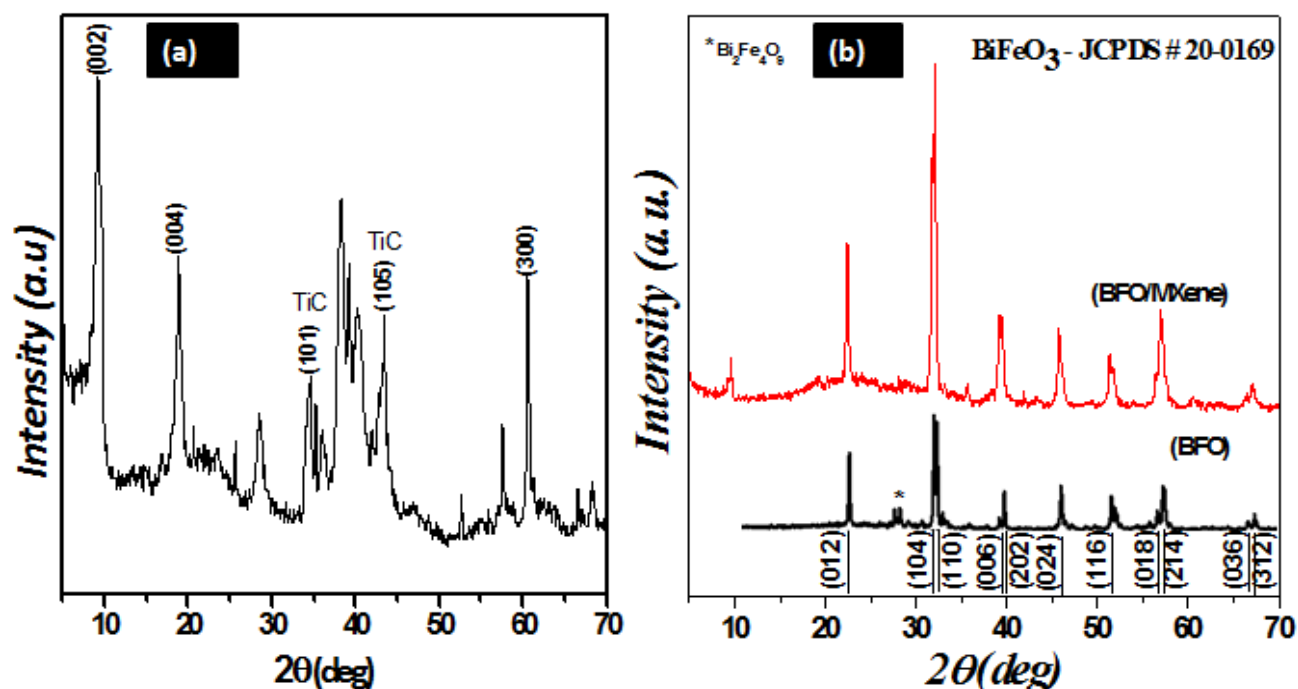


Figure 4.1.1. (a) X-Ray diffraction (XRD) of Pure MXene, (b) Pure BFO and BFO/MXene hybrid.

The XRD pattern of pure MXene is shown in Figure 4.1.1 (a). It is to be mentioned that the main peaks of MXene are of 002, and 004 planes. The peak at 9.38° indicates the removal of Aluminum from its MAX compound because the peak shifted from 9.7° towards lower angle 9.38° due to the increase in interplanar distance between the planes. The peaks at 9.4° and 19° correspond to the (002) and (004) planes [53, 54]. Whereas the intensity of the peak at an angle of 39° strongly reduced due to crystallinity and structural loss that takes place due to etching of Aluminum [53,54]. Figure 4.1.1 (b) shows the XRD of BFO nanoparticles and BFO/MXene hybrid. The peaks of BFO/MXene hybrid are broadened as compare to BFO nanoparticles due to the incorporation of MXene sheets that has lower periodicity after Aluminum etching [65]. The particle size of pure BFO and BFO/MXene hybrid are of 60 nm.

4.1.2. Scanning electron microscope (SEM)

The SEM images of Pure MXene and BFO/MXene hybrid are shown in Figure 4.1.2 (a, b) and the BFO/MXene hybrid shown in Figure 4.1.2 (c, d), respectively. In Figure 4.1.2 (a, b), it is shown there is a clear splitting seen in the MXene sheets after removal of Aluminum between the sheets. Figure 4.1.2, (c, d) shows that the BFO particles are attached to the MXene sheets rather than to penetrate it. The attachment of BFO nanoparticles on MXene sheets is a surface adsorption phenomenon. The attached BFO nanoparticles are irregular in shape and are spread on MXene sheets.

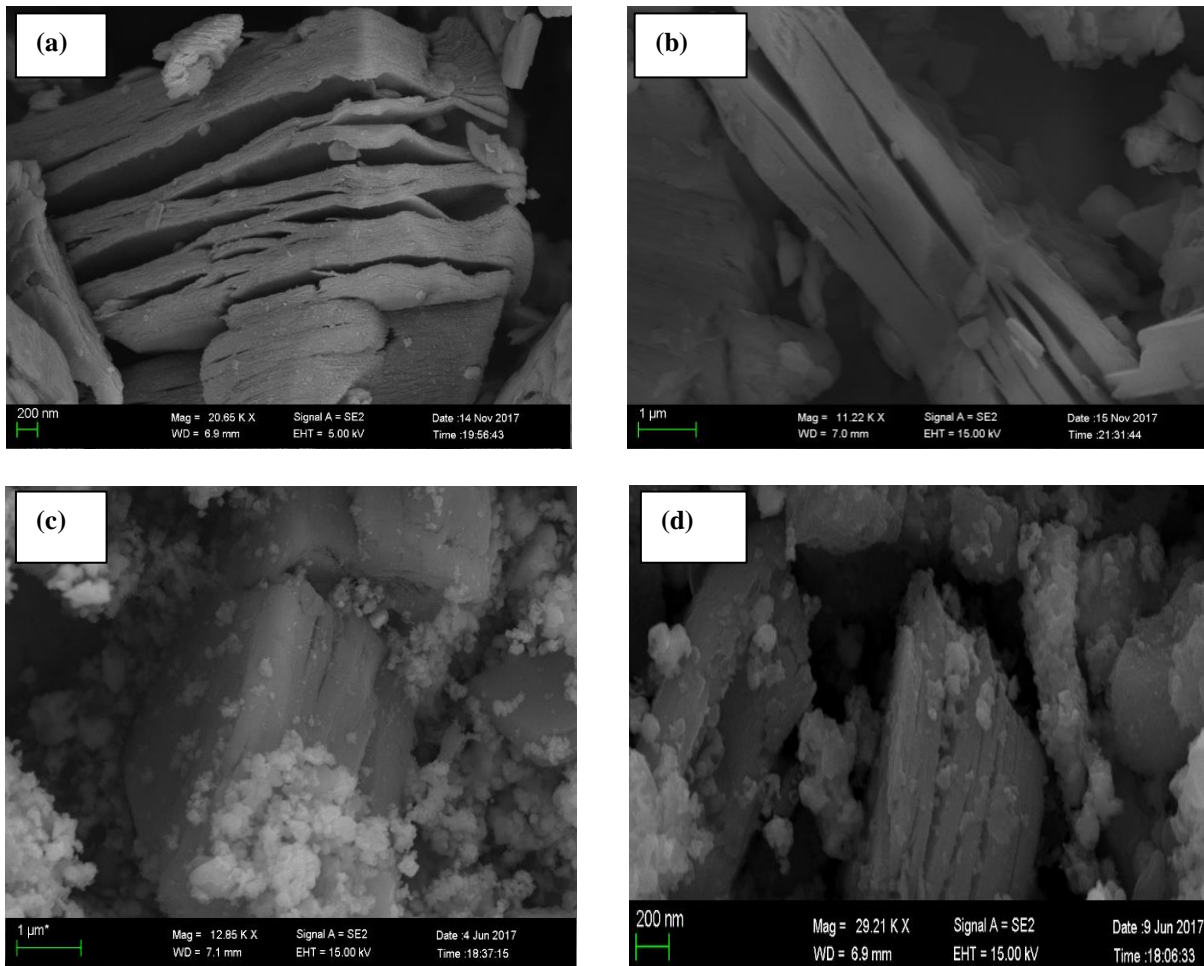


Figure 4.1.2. (a, b) show the morphology of etched MXene sheets, (c, d) show the morphology of BFO/MXene hybrid.

4.1.3. Energy Dispersive X-ray spectroscopy (EDXS)

Figure (4.1.3) shows the EDXS analysis of Pure MXene. It can be clearly seen that the Titanium (Ti), Carbon (C) with Oxygen and Fluoride functional group attached are present and the Aluminum (Al) signature due to partly etching of Ti_3C_2 from Ti_3AlC_2 powder observed in Figure 4.1.3. The platinum element is due to the platinum coating before the EDXS analysis of the sample.

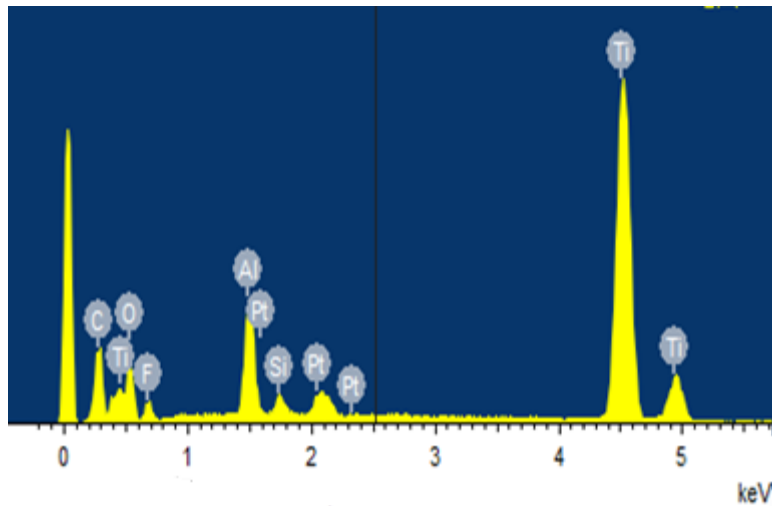


Figure 4.1.3. EDX of MXene

4.1.4. X-Ray Photoelectron Spectroscopy

Figure 4.1.4 (a) shows the survey spectrum of BFO/MXene hybrid. The survey spectrum indicates the presence of Bi, Fe, O, Ti and C in the prepared sample. Figure (b) shows that the peaks at 158 e.V and 164 e.V correspond to the Bi^{3+} peaks and there is no chemical shift takes place in case of Bi^{3+} element. Figure (c) shows the peaks of Fe 2p. The peak appeared at 710 e.V and 716 e.V are the Fe $2p_{3/2}$ and Fe $2p_{1/2}$ peak whereas the peak appeared at 724 e.V are the Fe_2O_3 peak with greater binding energy as compare to Fe^{+3} metallic peaks. Figure (d) shows that the peak at 532 e.V was the surface adsorbed Oxygen atom peak. The peaks of Titanium shown in Figure (e) are also at its exact position. The peak at 465 e.V was the Titanium oxide peak (TiO_2) and the two peaks appeared at 455 e.V and 462 e.V was the Ti $2p_{3/2}$ and Ti $2p_{1/2}$ peaks having an Oxidation state of (+4) [66, 67]. In Figure (f) the peak at the position of 284.8 e.V was the C-O peak [68].

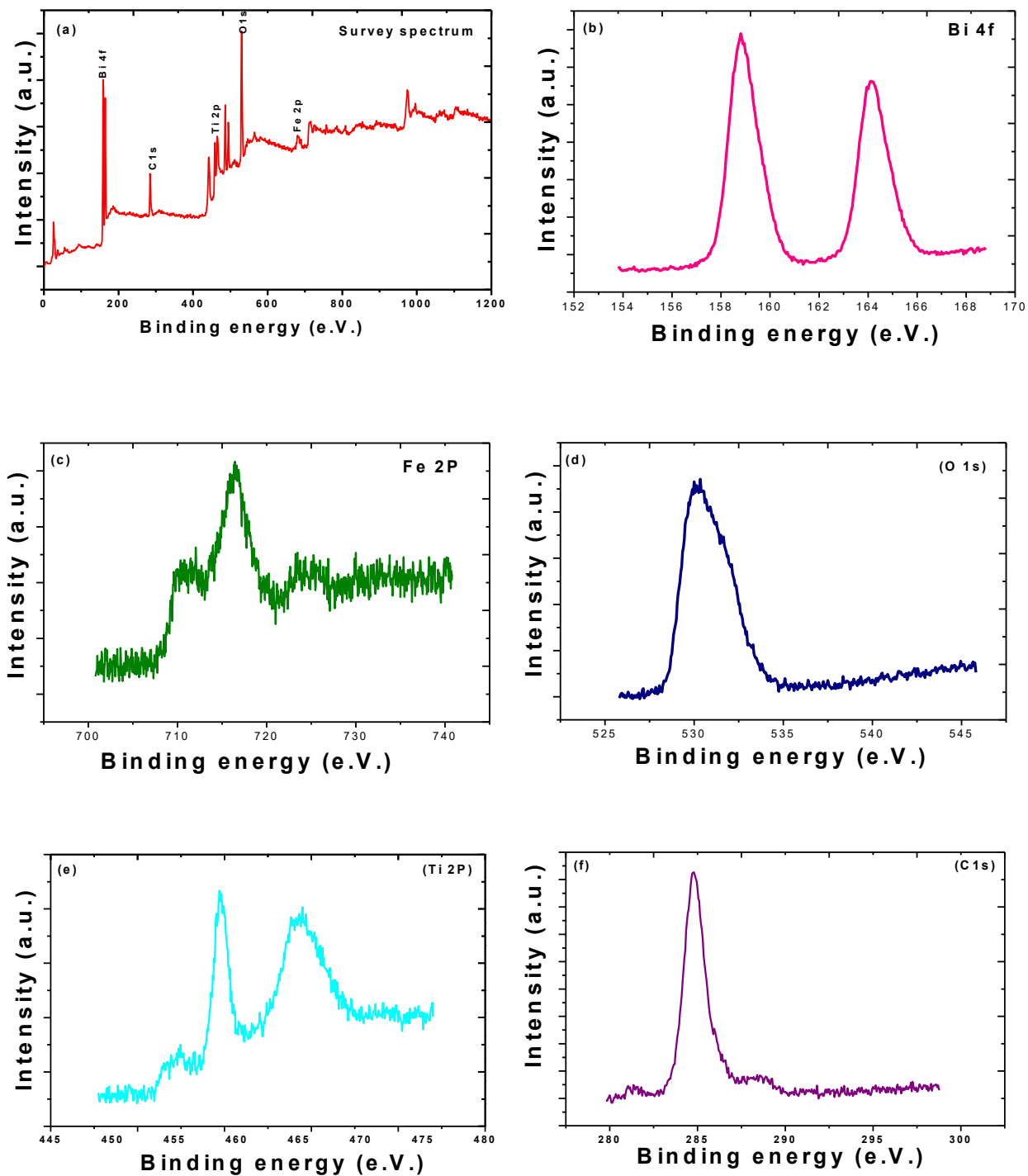


Figure 4.1.4. XPS analysis (a) Survey spectrum of BFO/MXene (b) Bi 4f core levels (c) Fe 2p core levels (d) O 1s core levels (e) Ti 2p core levels (f) C 1s core levels.

4.1.5. Photoluminescence Spectra (PL)

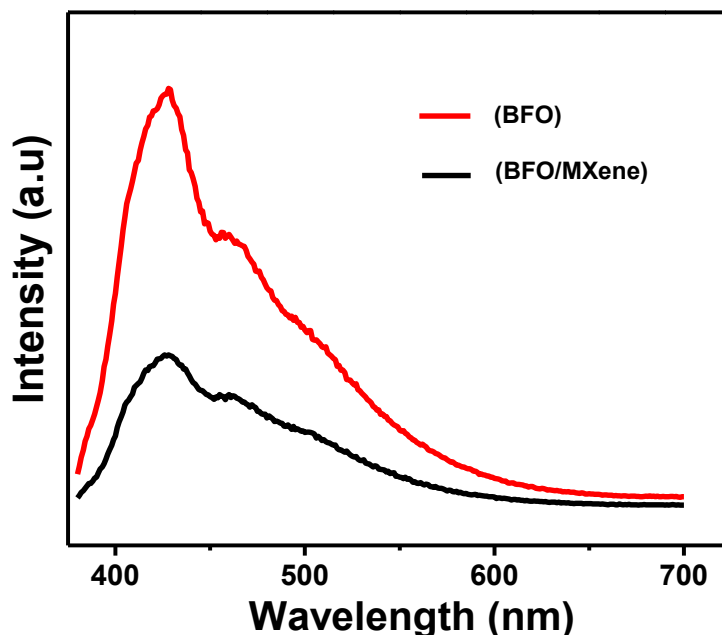


Figure 4.1.5. PL spectrum of BFO and BFO/MXene

Figure 4.1.5 shows the PL spectrum of pure BFO and BFO/MXene hybrid. The red peak indicates PL spectra of pure BFO and black peak shows the PL spectra of BFO/MXene. From PL spectra it is observed that the peak of high intensity corresponds to large electron-hole recombination rate whereas the lower peak intensity shows the low electron-hole recombination [68]. The pure BFO contains large electron-hole recombination hence, fewer radicals (OH^\cdot , O_2^\cdot) are produced for dye degradation and it lowers the photocatalytic activity. On the other hand, BFO/MXene shows low electron-hole recombination hence more radicals will be generated which enhance the dye degradation activity. The lower electron-hole recombination in the case of BFO/MXene is due to the presence of MXene sheets that provide a path for electrons to reside over its surface and thus, enhance the electron-hole recombination time.

4.1.6. Photocatalytic activity

4.1.6.1 Photocatalytic process for Dye Degradation

The photocatalytic process for dye degradation depends upon the generation of charge carriers upon light irradiation, reduction of electrons and oxidation of holes. The whole photocatalytic

process for dye degradation using BFO/MXene is shown in Figure 4.1.6. Figure 4.1.6, visible light interacts with the surface of BFO/MXene that generates electrons and holes. The electrons reached to the surface of a catalyst (BFO/MXene) and interact with the adsorbed Oxygen and reduce it into superoxide radicals (O_2^-); holes, on the other hand, react with water (H_2O) and reduce it into hydroxyl radicals (OH^\cdot). The O_2^- and OH^\cdot radicals are highly reactive species, both react with dye molecules and degrade it to give the end products (CO_2 & H_2O). The photocatalytic process in the form of the equation is given below [41, 42]:

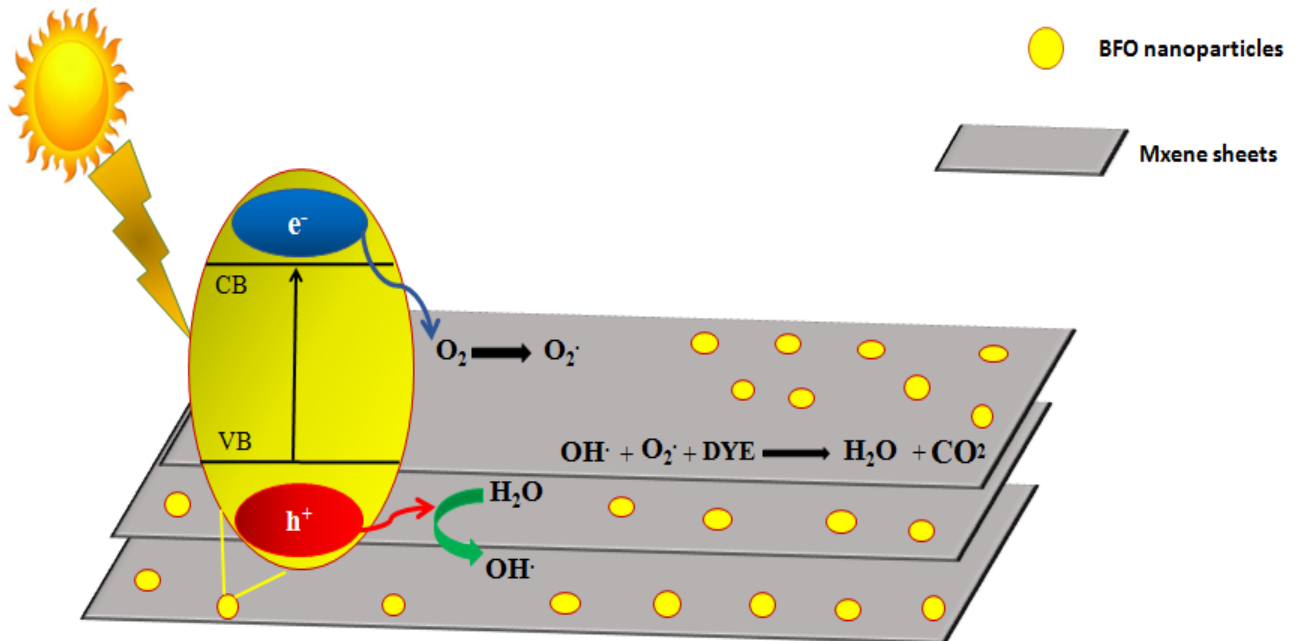
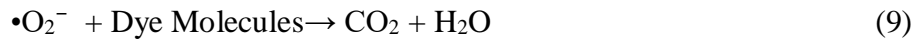
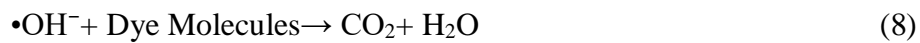
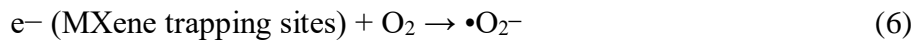
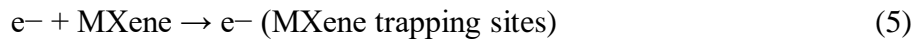


Figure 4.1.6. Photocatalytic process for Dye Degradation

4.1.6.2 Photocatalytic Activity of BFO/MXene

For the measurement of the photocatalytic activity of BFO and BFO/MXene the UV-visible spectrophotometer technique was used. The absorbance spectra for dye degradation at different times and photocatalytic activity of BFO/MXene are shown in Figure 4.1.7.

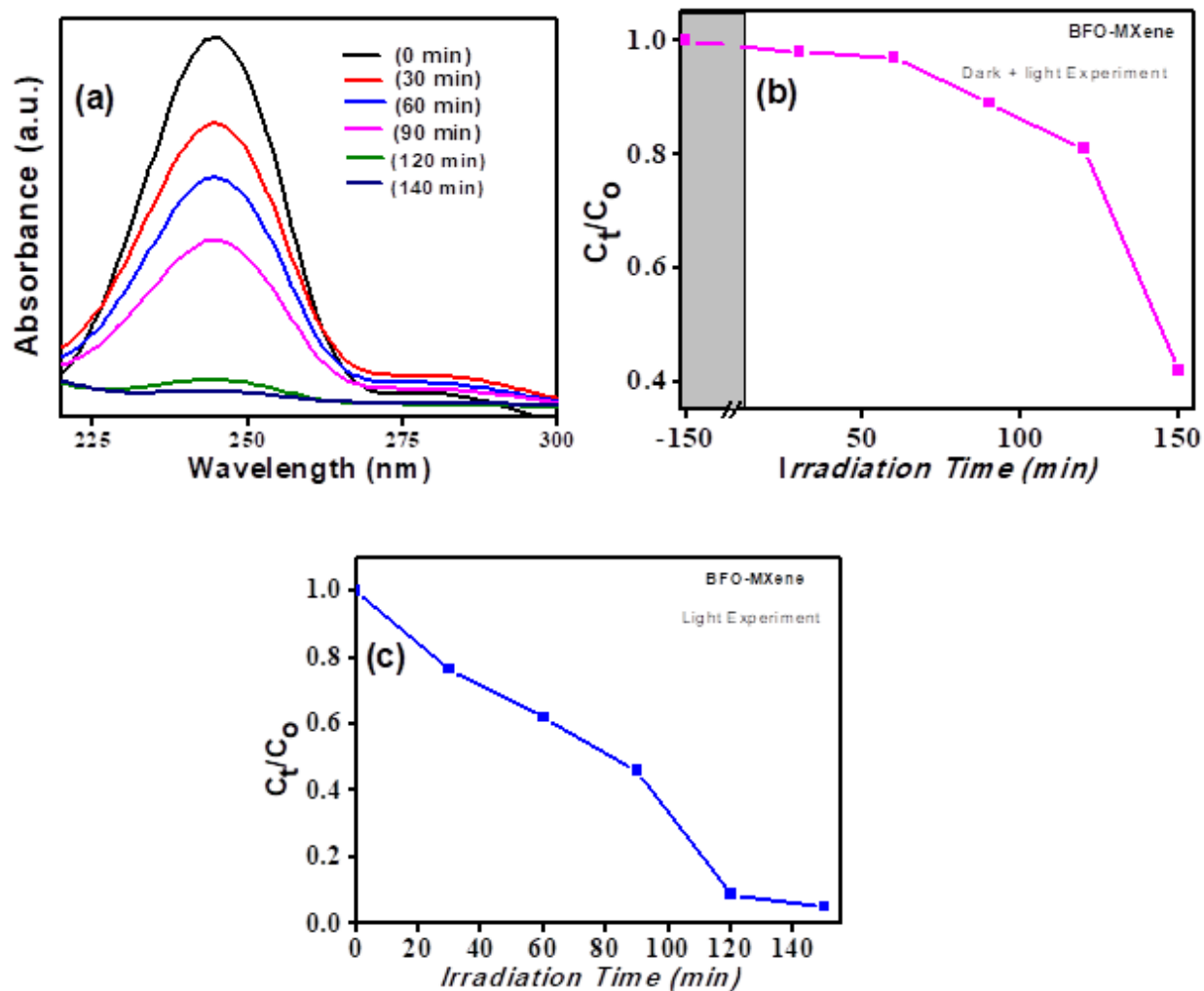


Figure 4.1.7. (a) The absorbance spectra of BFO/MXene shows the degradation efficiency of dye from solution at the different time (b) Photocatalytic degradation efficiencies of Acetophenone in the presence of BFO/MXene photocatalyst under dark experiment (c) Photocatalytic degradation efficiency of Acetophenone in the presence of BFO/MXene under light experiment.

Figure 4.1.7 (a) shows the degradation efficiency of acetophenone dye at a different time. With the passage of time the dye degraded from the catalytic solution because the concentration of dye molecules in the solution goes to decrease hence less light interacts and absorbs into dye molecules and shows the degradation of dye from a solution by the decrease of peak intensity, and

a time comes when dye completely degrades from the solution and peak intensity is reduced abruptly. At 0 minutes the maximum concentration of dye molecules is observed by the highest peak intensity but with the passage of time the peak intensity reduces and at 140 minutes the sharp reduction of peak intensity takes place, this is the clear indication of dye degradation from a catalytic solution.

The dark and light experiments were performed for the photocatalytic activity. A dark experiment was performed for the more adsorption of dye molecules on the surface of the catalysts and it shows 60% degradation of acetophenone under dark effect from the solution and shown in Figure. 4.1.7 (b). In dark the degradation of dye occurs because of the functional groups attached to MXene sheets. These functional groups provide reactive sites for degrading the molecules. When the catalyst surface was irradiated with visible light having a suitable wavelength then the photocatalyst causes to break down the acetophenone and it was completely degraded from the solution in about 140 minutes, as shown in Figure. 4.1.7 (c). Acetophenone is difficult to degrade as compared to other dyes like Congo red (CR) and methyl violet etc due to the highly stable benzene ring in its structure. The complete degradation rate of acetophenone was almost due to the enhanced properties of BFO/MXene hybrid formation.

CHAPTER 5 Results and Discussion-II

5.1. Part B: Sn and Gd-doped BFO (BGFSO/MXENE) Hybrid

5.1.1. X-Ray Diffraction (XRD)

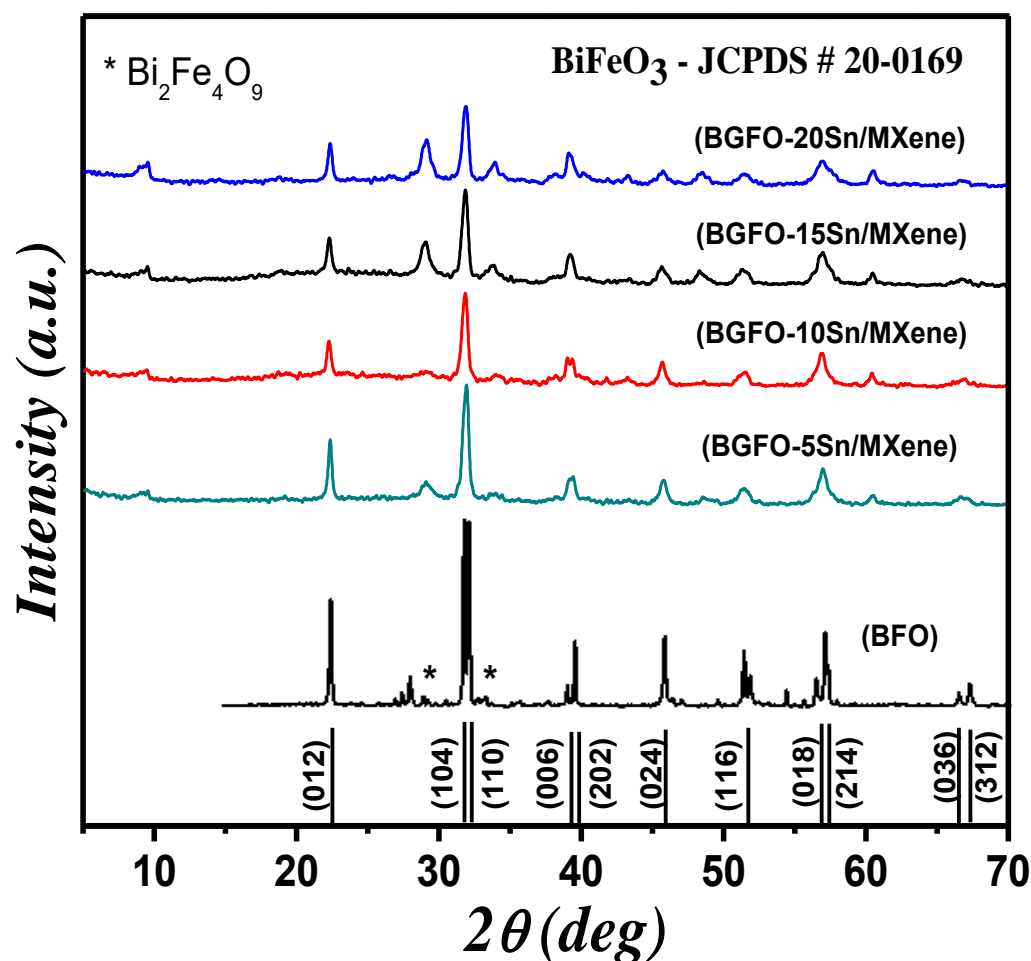


Figure 5.1.1. X-Ray diffraction (XRD) of Bi_{1-x}Gd_xFe_{1-y}Sn_yO₃ (x=0.1, y=0.0, 0.05, 0.10, 0.20)/MXene hybrid.

The XRD peaks of hybrids of (Bi_{0.90}Gd_{0.10}Fe_{0.95}Sn_{0.05}; BGFO-5Sn)/MXene, (Bi_{0.90}Gd_{0.10}Fe_{0.90}Sn_{0.10}; BGFO-10Sn)/MXene, (Bi_{0.90}Gd_{0.10}Fe_{0.85}Sn_{0.15}; BGFO-15Sn)/MXene and (Bi_{0.90}Gd_{0.10}Fe_{0.80}Sn_{0.20}; BGFO-20Sn)/MXene are shown in Figure 5.1.1. All the (hkl) peaks of BFO/MXene hybrid are matches with JCPDS card no 20-0169. The pure BFO has

rhombohedral structure at room temperature. The doping of Sn in BFO nanoparticles shift the doublet peak having plans of (104) and (110) into a sharp singlet peak and shows the structural transformation from Rhombohedral to Orthorhombic. The peak intensity of $\text{Bi}_2\text{Fe}_4\text{O}_9$ increases with the increase of Sn concentration [41]. The average particle size of (BFO, BGFO-5Sn, BGFO-10Sn, BGFO-15Sn, and BGFO-20Sn)/MXene hybrid are calculated using Scherer's equation ($D = K\lambda / \beta \cos\theta$) and it is 60 nm, 19.72 nm, 21.54 nm, 20.8 nm, 20.96 nm respectively. The main XRD peaks of doped BFO and MXene are present in all the hybrid samples. All the XRD peaks in hybrid samples are broadened and have low peak intensity than that of pure BFO.

5.1.2. SEM Analysis

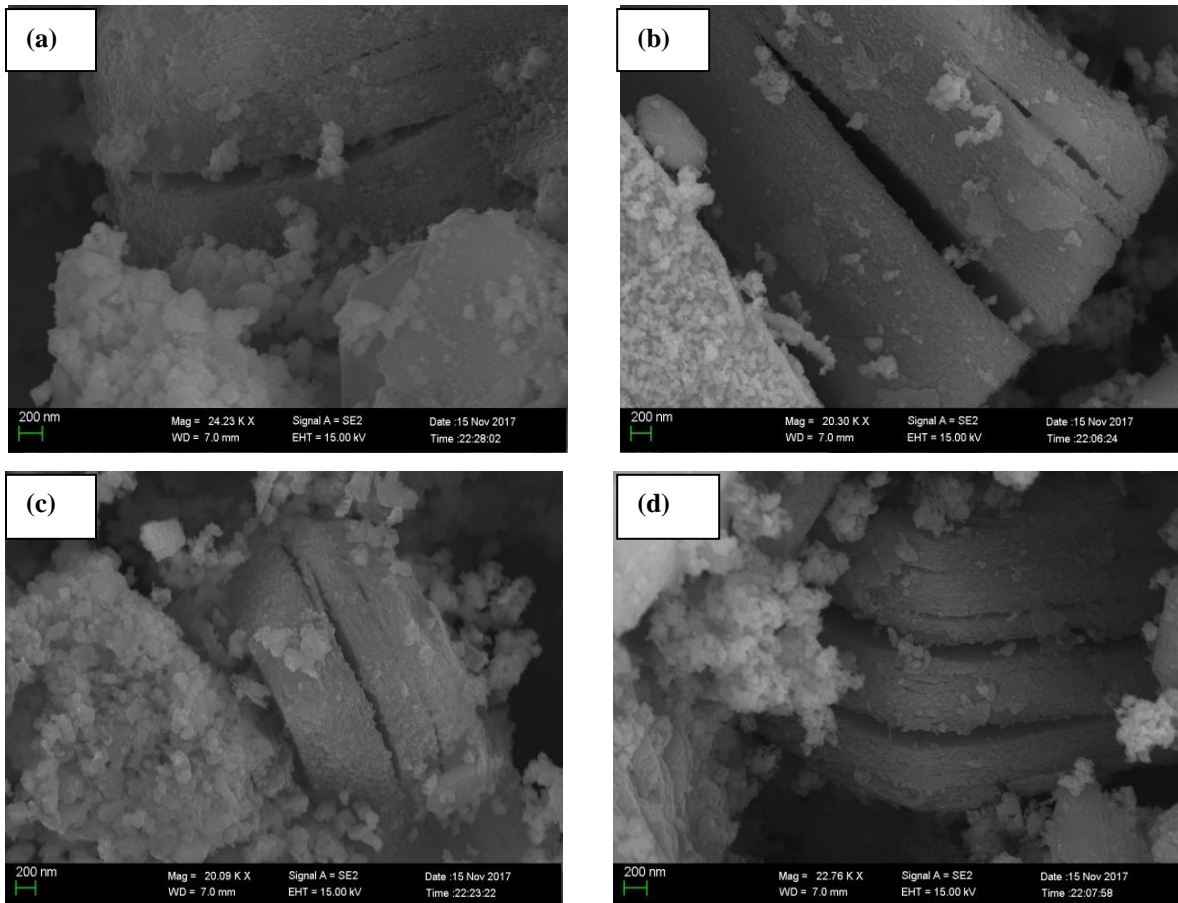


Figure 5.1.2. SEM images of doped BFO/MXene hybrid (a: Sn= 5%, b: 10%, c: 15%, d: 20%).

From figure 5.1.2 it can be seen that the BGFSO nanoparticles are attached on the MXene sheets and it does not embed onto the MXene sheets that are the clear indication of a physical mixing between two species that form hybrid structures. With the doping concentration of Sn (5 %, 10 %, 15 %, and 20 %) the nanoparticles become agglomerate. From the figure 5.1.2, the clear white color indicates the agglomeration of nanoparticles. Due to agglomeration, the less number of BGFSO nanoparticles covered the MXene sheets.

5.1.3. The Bandgap of MXene

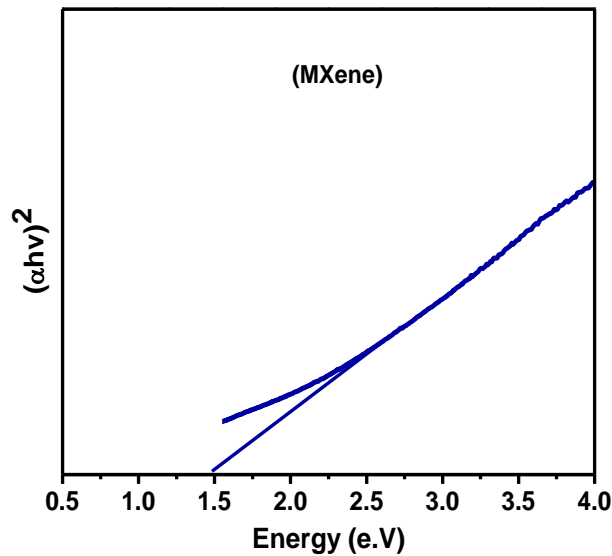


Figure 5.1.3. The Bandgap of pure MXene

The band gap of MXene was checked by using a UV-visible spectrophotometer. From figure 5.1.3 it is clear that MXene sample are continuously absorb the light and no absorption edge appeared in Figure 5.1.3 due to the metallic nature of etched MXene powder [54, 55]. The band gap of MXene was estimated by plotting $(\alpha h\nu)^2$ against the band gap energy (E_g) and a straight line appeared that is extrapolated towards x-axis and the point at which the line meets with x-axis that point is the band gap of the required sample [39]. The band gap of MXene was found to be 1.5 e.V [36].

5.1.4. Photoluminescence spectra of BGFSO/MXene hybrid

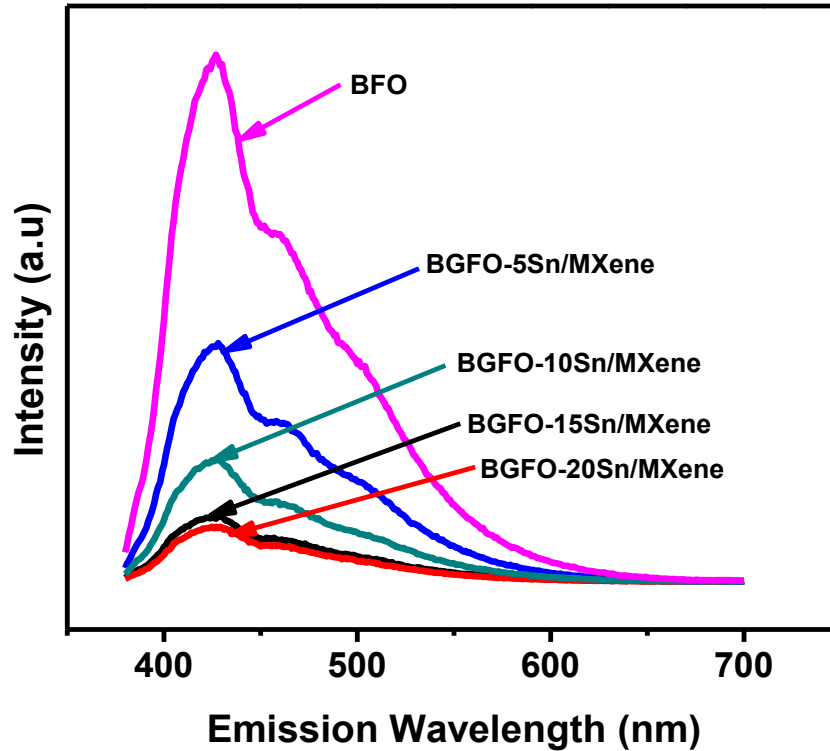


Figure 5.1.4. PL spectra of BGFSO/MXene hybrid

Figure 5.1.4 shows the Photoluminescence (PL) emission spectra for BGFSO/MXene hybrid. The photoluminescence (PL) spectra having a central peak at the position 426 nm and the shoulder peak at 458 nm. The central emission peak appeared at 426 nm shows the electron-hole recombination rate, the greater the electron-hole recombination rate greater will be the PL peak intensity and vice versa [42]. From Figure 5.1.5 it is clearly observed that the red and black peaks correspond to BGFO-20Sn/MXene and BGFO-15Sn/MXene hybrid sample having small PL peak intensity that indicates the low electron-hole recombination than that of BFO/MXene, BGFO-5Sn/MXene, and BGFO-10Sn/MXene. The low PL peak corresponds to better photocatalytic activity due to the wide range of charge separation.

5.1.5. Photocatalytic activity of BGFSO/MXene hybrid samples

The dye absorbance spectra of BFO/MXene, BGFO-5Sn/MXene, BGFO-10Sn/MXene, BGFO-15Sn/MXene, BGFO-20Sn/MXene and pure MXene are shown in Figure 5.1.5 (a-e). The absorbance spectra provide information about the degradation efficiency of Congo red dye from the catalytic solution at a different time [41]. The black peak in all Figures (a-e) shows the highest concentration of dye molecules in the solution. The decrease of absorbance peak intensity at a different time is the clear indication of dye degradation from the catalytic solution. After 30 minutes the peaks of pure MXene is shifted towards the longer wavelength side because of the oxidization of MXene sheets ($Ti_3C_2O_2$) [69-73]. In Figure 5.1.5 (f) the black line corresponds to the degradation of Congo red from the solution under blank experiment. Figure 5.1.5 (f) shows the photocatalytic activity of pure MXene and BGFSO/MXene hybrid and it is checked that 80% of Congo red dye degraded from pure MXene solution in only 120 minutes, BGFO-5Sn degraded 38% of Congo red dye, whereas 18% dye degradation takes place from the BGFO-10Sn and BGFO-15Sn in 120 minutes. The BGFO-20Sn shows the 100% dye degradation in 120 minutes.

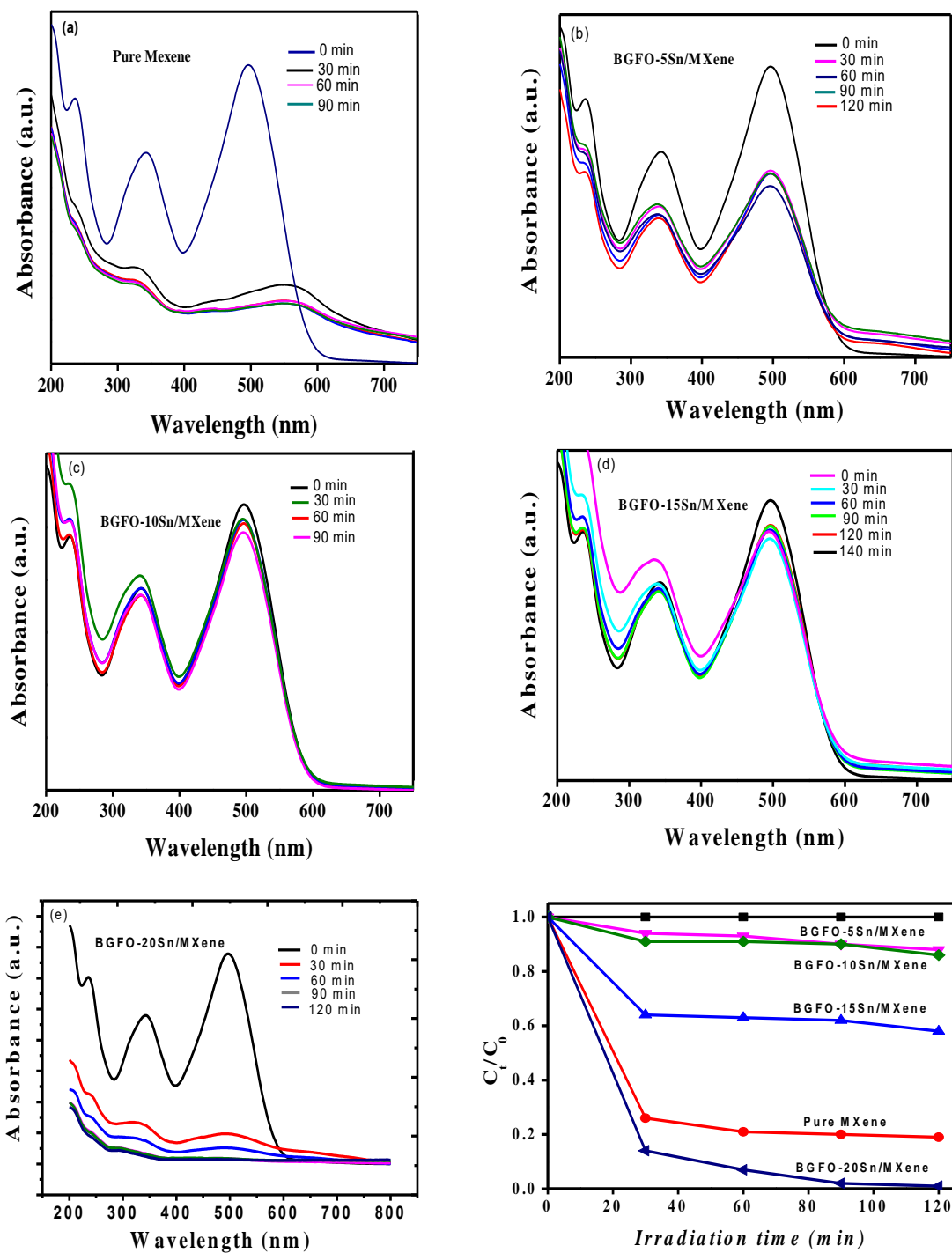


Figure 5.1.5. (a-e) The absorbance spectra of Pure MXene, BGFO-5Sn/MXene, BGFO-10Sn/MXene, BGFO-15Sn/MXene and BGFO-20Sn/MXene hybrid sample. (f) Photocatalytic degradation of Pure MXene, BGFO-5Sn/MXene, BGFO-10Sn/MXene, BGFO-15Sn/MXene and BGFO-20Sn/MXene hybrid samples.

Conclusion

The BFO nanoparticles were fabricated by the simple sol-gel method. The 2D MXene sheets were obtained by the etching of Aluminum from MAX compound. The etching was performed using Hydrofluoric acid (HF). The hybrid of BFO/MXene was synthesized by Co-precipitation method. The obtained hybrid was characterized by XRD, SEM, XPS, and UV-visible. The BFO/MXene hybrid was used for the degradation of Acetophenone and it was observed that 100% degradation of Congo red was taken place. This indicates that BFO/MXene is a good photocatalyst. Whereas the hybrid of Gadolinium (Gd) and Tin (Sn) doped BFO nanoparticles with MXene sheets also a good catalyst. The degradation rate of Congo red dye from the catalytic solution of $(\text{Bi}_{0.90}\text{Gd}_{0.10}\text{Fe}_{0.80}\text{Sn}_{0.20}$; BGFO-20Sn)/MXene is 100%, whereas the $(\text{Bi}_{0.90}\text{Gd}_{0.10}\text{Fe}_{0.95}\text{Sn}_{0.05}$; BGFO-5Sn)/MXene shows 38% degradation, $(\text{Bi}_{0.90}\text{Gd}_{0.10}\text{Fe}_{0.90}\text{Sn}_{0.10}$; BGFO-10Sn)/MXene and $(\text{Bi}_{0.90}\text{Gd}_{0.10}\text{Fe}_{0.85}\text{Sn}_{0.15}$; BGFO-15Sn)/MXene shows 18% degradation. The photocatalytic activity depends on the adsorption and degradation of dye from the solution. The good photocatalyst results show that the pure and doped BFO/MXene hybrid is a potential candidate for various commercial applications.

References

1. Society, R., *Nanoscience, and Nanotechnologies: Opportunities and Uncertainties: Summary and Recommendations*. Royal Society: **2004**.
2. Speshock, J. L.; Murdock, R.C.; Braydich- Stolle, L.K.; Schrand, A.M.; Hussain, S.M., Interaction of Silver nanoparticles with the Tacarible virus. *Journal of Nanobiotechnology* **2010**, 8 (1), 19.
3. Anischik V. M., Borisenko V.E., Zhdanok S.A., Tolochko N.K., Fedosyuk V.M., *Nanomaterials and Nanotechnologies: Minsk: 2008*.
4. Borisenko V.E., Tolochko N.K., *Nanotechnologies: Stages of Development*. Nauka i innovatsii Minsk: **2008**, 66-68.
5. Foster L., *Nanotechnology Science: Minsk: 2005*.
6. Poole C. Jr., Owens F., *Introduction to Nanotechnology: Wiley: 2003*.
7. Roko M.C., Williams R.S., Alivisatos P., *Nanotechnology Research Directions: Vision for Nanotechnology in the Next Decade*. New York, Springer: **2000**.
8. Luisa F., Duncan S., *Fundamental concepts in Nanoscience and nanotechnologies: Inano: 2010*.
9. Arivalagan K.; Ravichandran S.; Rangasamy K.; Karthikeyan E., Nanomaterials and its potential applications. *Int. J. Chem Tech Res* **2011**, 3 (2), 534-538.
10. Sajanlal P R., Sreeprasad T S., Samal A K., Pradeep T., *Introduction to Nanomaterials 2011*.
11. Jitendra N., Rajanish N., Kwang S ., *Progress in Material Science* **2012**, 8, 724-803.
12. Feng, L.; Liu, Z., Graphene in biomedicine: opportunities and challenges. *Nanomedicine* **2011**, 6 (2), 317-324.
13. Suzuki, M.; Kawamura, N.; Miyagawa, H.; Garitaonandia, J.S.; Yamamoto, Y.; Hori, H., Measurement of a Pauli and orbital paramagnetic state in bulk gold using x-ray magnetic circular dichroism spectroscopy. *Physical Review Letters* **2012**, 108 (4), 047201.
14. Besner, S.; Meunier, M., Laser synthesis of nanomaterials. *Laser Precision Microfabrication* **2010**, 135, 163-188.
15. Mlinar, V., Engineered nanomaterials for solar energy conversion. *Nanotechnology* **2013**, 24 (4), 042001.

16. Lebeugle, D.; Colson, D.; Forget, A.; Viret, M.; Bonville, P.; Marucco, J.F.; Fusil, S., Room temperature coexistence of large electric polarization and magnetic order in BiFeO₃ single crystals. *Physical Review B* **2007**, 76 (2), 024116.
17. Wen, Z.; Hu, G.; Fan, S.; Yang, C.; Wu, W.; Zhou, Y.; Chen, X.; Cui, S., Effects of annealing process and Mn substitution on the structure and ferroelectric properties of BiFeO₃ films. *Thin Solid Films* **2009**, 517 (16), 4497-4501.
18. Gupta, S.; Sharma, A.; Tomar, M.; Gupta, V.; Pal, M.; Guo, R.; Bhalla, A., Piezoresponse force microscopy and vibrating sample magnetometer study of single-phased Mn-induced multiferroic BiFeO₃ thin film. *Journal of Applied Physics* **2012**, 111 (6), 064110.
19. Park, T.J.; Papaefthymiou, G.C.; Viescas, A.J.; Moodenbaugh, A.R.; Wong, S.S.; Size-dependent magnetic properties of single crystalline multiferroic BiFeO₃ nanoparticles. *Nano Letters* **2007**, 7 (3), 766-772.
20. Seshadri, R.; Hill, N.A., Visualizing the role of Bi 6s “lone pairs” in the off-center distortion in ferromagnetic BiMnO₃. *Chemistry of Materials* **2001**, 13 (9), 2892-2899.
21. Wang, K.F., Liu, J.M., Ren, Z.F., “Multiferroicity: the coupling between magnetic and polarization orders”, *Adv. Phys* **2009**, 58, 321.
22. Sharma, S.; Singh, V.; Kotnala, R.; Dwivedi, R.K., Comparative studies of pure BiFeO₃ prepared by sol-gel versus conventional solid state reaction method. *Journal of Material Science: Materials in Electronics* **2014**, 25 (4), 1915-1921.
23. Yang, C.H., Kan, D., Takeuchi, I., Nagarajan, V., Seidel, J., “Doping BiFeO₃ approaches and enhanced functionality”, *Phys. Chem. Chem. Phys* **2012**, 14, 15953.
24. Mocherla, P.s.; Karthik, C.; Ubic, R.; Ramachandra Rao, M.; Sudhakar, c., the Tunable band gap in BiFeO₃ nanoparticles: the role of microstrain and oxygen defects. *Applied Physics Letters* **2013**, 103 (2), 022910.
25. Buscaglia, M. T., Mitoseriu, L., Pellechi, L., Buscaglia, V., Viviani, M., Siri, A.S., Preparation and characterization of the magneto-electric xBiFeO₃-(1-x)BaTiO₃ ceramics”, *J. Eur. Ceram. Soc* **2006**, 26, 3027.
26. Lahmara, A., Zhao, K., Habouti, S., Dietze, M., Solterbeck, C.H., Sounia M.Es., “Off stoichiometry effects on BiFeO₃ thin films”, *Solid State Ionics* **2011**, 202, 1.

27. Das, S., Basu, S., Mitra, S., Chakravorty, D., Mondal, B.N., “Wet chemical route to transparent BiFeO₃ films on SiO₂ substrates”, *Thin Solid Films* **2010**, 518, 4071.
28. Kumar, M. M., Palker, V. R., Srinivas, K., Suryanarayana, S. V., “Ferroelectricity in pure BiFeO₃ ceramics”, *Appl. Phys. Lett* **2000**, 76, 2764.
29. Palai, R., Katiyar, R. S., Schmid, H., Tissot, Clark, S. J., Robertson, J., Redfern, S. A. T., Catalan, G., Scott, J. F., “ β phase and γ - β metal-insulator transition in multiferroic BiFeO₃”, *Phys. Rev. B* **2008**, 77, 014110.
30. Sanguansri, P.; Augustin, M.A., Nanoscale materials development a food industry perspective. *Trends in Food Science and Technology* **2006**, 17 (10), 547-556.
31. Zhang, M.; Dai, L., Carbon nanomaterials as metal-free catalysts in next-generation fuel cells. *Nano Energy* **2012**, 1 (4), 514-517.
32. Aguilar, Z.P.; Aguilar, Y.; Xu, H.; Jone, B.; Dixon, J.; Xu, H.; Wang, Y.A., Nanomaterials in medicine. *ECS Transactions* **2010**, 33 (8), 69-74.
33. Morris, V., Emerging roles of engineered nanomaterials in the food industry. *Trends in Biotechnology* **2011**, 29 (10), 509-516.
34. Jariwala, D.; Sangwan, V.K.; Lauhon, L.J.; Marks, T.J.; Hersam, M.C., Carbon nanomaterials for electronics, optoelectronics, photovoltaics, and sensing. *Chemical Society Reviews* **2013**, 42 (7), 2824-2860.
35. Eerenstein, W.; Mathur, N.; Scott, J.F., Multiferroic and magnetoelectric materials. *Nature* **2006**, 442, 7104, 759.
36. Shun Li, Yuan-Hua Lin, Bo-Ping Zhang, Ce-Wen Nan, and Yao Wang, Photocatalytic and magnetic behaviors observed in nanostructured BiFeO₃ nanoparticles. *Journal of Applied Physics* **2009**, 105, 056105.
37. Renqing Guo, Liang Fang, Wen Dong, Fengang Zheng, and Mingrong Shen., Enhanced Photocatalytic Activity and Ferromagnetism in Gd Doped BiFeO₃ Nanoparticles. *J. Phys. Chem. C* **2010**, 114, 21390–21396.
38. Jian He, Renqing Guo, Liang Fang, Wen Dong, Fengang Zheng, Mingrong Shen, Characterization and visible light photocatalytic mechanism of size-controlled BiFeO₃ nanoparticles. *Journal of American chemical society (ACS)* **2013**, 48, 3017-3024.

39. Mohan, S.; Subramanian, B, Bhaumik, I.; Gupta, P.K.; Jaisankar, S.n., Nanostructured Bi_(1-x)Gd_(x)FeO₃ a multiferroic photocatalyst on its sunlight-driven photocatalytic activity. *RSC Advances* **2014**, 4 (32), 16871-16878.
40. Syed Irfan, Yang Shen, Syed Rizwan, Huan-Chun Wang, Sadaf Khan, Ce-Wen Nan.; Band-gap engineering and enhanced photocatalytic activity of Sm and Mn-doped BiFeO₃ nanoparticles. *J Am Ceram Soc* **2016**, 100, 31- 40.
41. Irfan, S. *et al.* The Gadolinium (Gd³⁺) and Tin (Sn⁴⁺) Co-doped BiFeO₃ Nanoparticles as New Solar Light Active Photocatalyst. *Sci. Rep* **2017**, 7, 42493.
42. Syed Irfan, Liangliang Li, Awais Siddique Saleemib and Ce-Wen Nana.; the Enhanced photocatalytic activity of La³⁺ and Se⁴⁺ co-doped bismuth ferrite nanostructures. *J. Mater. Chem. A* **2017**, 5, 11143.
43. Christelle Pau Ping Wong, Chin Wei Lai, Kian Mun Lee and Sharifah Bee Abd Hamid.; Advanced Chemical Reduction of Reduced Graphene Oxide and Its Photocatalytic Activity in Degrading Reactive Black 5. *Materials* **2015**.
44. Yongye Liang, Hailiang Wang, Hernan Sanchez Casalongue, Zhuo Chen and Hongjie Dai. TiO₂ Nanocrystals Grown on Graphene as Advanced Photocatalytic Hybrid Materials. *Springer* **2010**, 8, 7118–7128.
45. Yongsheng Fu, Qun Chen, Mingyang He, Yunhai Wan, Xiaoqiang Sun, Hui Xia, and Xin Wang.; Copper Ferrite-Graphene Hybrid: A Multifunctional Heteroarchitecture for Photocatalysis and Energy Storage. *Industrial & Engineering Chemistry Research* **2012**, 51, 11700–11709.
46. Li, Z.; Shen, Y.; Yang, C.; Lei, Y.; Gun, Y.; Lin, Y.; Liu, D.; Nan, C, W., Significant enhancement in the visible light photocatalytic properties of BiFeO₃-Graphene nanohybrids. *Journal of Materials Chemistry A* **2013**, 1 (3), 823-829.
47. Dai, J.; Xian, T.; Di, I.; Yang, H., Preparation of BiFeO₃- Graphene nanocomposites with their enhanced photocatalytic activities. *Journal of Nanomaterials* **2013**, 1.
48. Sun, H.; Liu, Y.; Zhang, Y.; Lv, L.; Zhou, j.; Chen, W., Synthesis of Bi₂Fe₄O₉-RGO composite by one step hydrothermal method and its high photocatalytic performance. *Journal of Materials Science: Materials in electronics* **2014**, 25 (10), 4212-4218.

49. Sun, A.; Chen, H.; Song, C.; Jiang, F.; Wang, X.; Fu, Y., Magnetic Bi₂₅FeO₄₀ Graphene catalyst and its high visible light photocatalytic performance. *RSC Advances* **2013**, 3 (13), 4332-4340.
50. Xingang Zhang, Bo Wang, Xiuzhang Wang, Xiangheng Xiao, Zhigao Dai, Wei Wu, k Junfeng Zheng, Feng Ren, and Changzhong Jiang., Preparation of M/BiFeO₃ Nanocomposites (M = Ag, Au) Bowl Arrays with Enhanced Visible Light Photocatalytic Activity, *J. Am. Ceram. Soc* **2015**, 98, 2255–2263.
51. Huidan Lu, Zhenyu Du, Jixiang Wang, Yongping Liu, the Enhanced photocatalytic performance of Ag-decorated BiFeO₃ in the visible light region, *Journal of Sol-gel Science and Technology* **2015**, 76, 50–57.
52. Muhammad Humayun, Amir Zada, Zhijun Li, Mingzheng, Xie, Xuliang Zhang, Yang Qu, Fazal Raziq, Liqiang Jing, Enhanced visible-light activities of porous BiFeO₃ by coupling with nanocrystalline TiO₂ and mechanism. *Applied Catalysis B environmental* **2016**, 180, 219-226.
53. Mashtalir, O.; Cook, K.M.; Mochalain, V.; Crowe, M.; Barsoum, M.W.; Gogotsi, Y., Dye adsorption and decomposition on two-dimensional titanium carbide in aqueous media. *Journal of Materials Chemistry A* **2014**, 2 (35), 14334-14338.
54. Chao Peng, Xianfeng Yang, Yuhang Li, Hao Yu, Hongjuan Wang, and Feng Peng., Hybrids of Two-Dimensional Ti₃C₂ and TiO₂ Exposing {001} Facets toward Enhanced Photocatalytic Activity. *American Chemical Society* **2016**, 8, 6051–6060.
55. Yupeng Gao, Libo Wang, Aiguo Zhou, Zhengyang Li, Jingkuo Chen, Hari Bala, Qianku Hu, Xinxin Cao., Hydrothermal synthesis of TiO₂/Ti₃C₂ nanocomposites with enhanced photocatalytic activity. *Materials Letters* **2015**, 150, 62–64.
56. L. F. Vassamillet *J. Appl. Phys.* **1969**, 40, 1637.
57. B. E. Warren X-ray Diffraction, Addison–Wesley **1969**.
58. E. W. Nuffield X-ray Diffraction Methods, Wiley **1966**.
59. Reichelt, R., Scanning electron microscopy. In *Science of Microscopy*, Springer: **2007**, 133-72.
60. G. R. Chatwal, S. K. An and Instrumental methods of chemical analysis, Himalaya Publishing House **1979**.
61. Weckhuysen, B.M., Ultraviolet-visible spectroscopy. **2004**.

62. Blake Wells, David McIntyre /Ph.D. Thesis / Oregon State University/ **2015**.
63. Nikita H. Patel / Ph. D. Thesis / Sardar Patel University/ July–**2015**.
64. Roger Smart, Stewart McIntyre, Mike Bancroft, Igor Bello/Department of Physics and Materials Science City University of Hong Kong, Surface Science Western, UWO.
65. S. Singh, H. Ishiwara, K. Maruyama., Formation of magnetite in Bismuth Ferrite under voltage stressing. *Applied Physics Letters* **2006**, 88, 262908.
66. G. Zou, Z. Zhang, J. Guo, B. Liu, Q. Zhang, C. Fernandez, Q. Peng., Fabrication of hierarchical MXene based AuNPs-containing core-shell nanocomposites for high efficient catalysts. *ACS Applied Materials & Interfaces* **2016**, 8, 22280.
67. Z. Zhang, H. Li, G. Zou, C. Fernandez, J. Hu, B. Liu, Q. Zhang, Q. Peng., Inorganic perovskite photocatalysts for solar energy utilization. *ACS Sustainable Chemistry & Engineering* **2016**, 45, 5951-5984.
68. T. Soltani, B.-K. Lee., Comparison of benzene and toluene photodegradation under visible light irradiation by Ba-doped BiFeO₃ magnetic nanoparticles with fast sonochemical synthesis. *Chemical Engineering Journal* **2016**, 306, 204.
69. I. Persson, L. Näslund, J. Halim, M. Barsoum, V. Darakchieva, J.Palisaitis, J. Rosen., Tailoring structure, composition, and Energy storage properties of MXene from selective etching of In-plane, chemically ordered MAX Phases. *IOP Publishing*. **2017**, 5, 015002.
70. E. Satheeshkumar, T. Makaryan, A. Melikyan, H. Minassian, Y. Gogotsi, M. Yoshimura., One-step solution processing of Ag, Au and Pd @ MXene Hybrids for SERS. *Scientific Reports* **2016**, 6, 32049.
71. G.R.Berdiyrov, Optical properties of functionalized Ti₃C₂T₂ (T= F, O, OH) MXene: First-principles calculations. *AIP Advances* **2016**, 6, 055105.
72. W. Feng, H. Luo, Y. Wang, S. Zeng, L. Deng, X. Zhou, H. Zhang, S. Peng., Ti₃C₂ MXene: a promising microwave absorbing the material. *RSC Advances* **2018**, 8, 2398-2403.
73. B. Balamurugana, T. Maruyama., Evidence of an enhanced interband absorption in Au nanoparticles: Size-dependent electronic structure and optical properties. *Applied Physics Letters* **2005**, 87, 143105.

